Realization of novel entangled photon sources using periodically poled materials

by

Deny R. Hamel

A thesis
presented to the University of Waterloo
in fulfillment of the
thesis requirement for the degree of
Master of Science
in
Physics

Waterloo, Ontario, Canada, 2010

I hereby declare that I am the sole author of this thesis. This is a true copy of the thesis, including any required final revisions, as accepted by my examiners.

I understand that my thesis may be made electronically available to the public.

Abstract

This thesis deals with the production of entangled photons using spontaneous parametric down-conversion (SPDC). We start with a short overview of some important theoretical concepts. First we provide a brief reminder of the theory of entanglement. We then discuss how the state of quantum systems can be determined using quantum state tomography. We also explain SPDC, the physical process which we use to produce entangled photons. Finally, we give an overview of the methods which have been used to produce entangled photons in the past, both for two- and three-photon entanglement.

The first experiment is the design of an efficient source of entangled photon pairs based on a polarizing Sagnac interferometer configuration. With this configuration, we can use quasi-phasematched materials which allow for higher efficiencies than standard bulk nonlinear materials. The source is pumped by a low-power continuous-wave laser diode, and produces degenerate photon pairs at 809nm. It has a spectral brightness of $87,500$ pairs/s $\cdot$ mW $\cdot$ nm, and the fidelity of the produced quantum states with a Bell state is 98.9%. The source is used for experiments in quantum key distribution, cluster state quantum computing, remote state preparation, state discrimination, and entanglement-enhanced classical communication.

The second experiment discussed in this thesis is the generation of photon triplets using cascaded SPDC. In this experiment, a primary SPDC source is pumped with a low-power, continuous-wave laser diode, producing photon pairs. Single photons from these pairs serve as the pump for a second down-conversion, resulting in photon triplets. This is the first demonstration of the direct production of photon triplets, and the first observation of SPDC at the single photon level. This method could potentially be used to produce entangled photon triplets without post-selection, and as a source of triggered Bell pairs.

Acknowledgements

I would first like to thank Kevin Resch, who has been a great supervisor over the last two years. I have benefited countless times from his availability, and his enthusiasm for research is contagious. I am excited to pursue my PhD under his supervision. I would also like to thank the other members of my advising committee, Thomas Jennewein and Donna Strickland. Thomas also played a key role in the cascaded SPDC experiment. I am very appreciative of his help during this project; I feel like he treated me as one of his own students. I also thank Norbert Lütkenhaus, who has accepted to be on my examining committee.

I would like to thank the other members of the Quantum Optics and Quantum Information group for their unconditional help in the lab. Of particular importance to my project was the help of Rainer Kaltenbaek, who beyond answering every one of my questions without complaint, has written many of the Labview programs which were used for this thesis. I would also like to mention Jonathan Lavoie and Devon Biggerstaff, who were always glad to give me advice on experimental methods, Kurt Schreiter for his help with Labview programming, and Robert Prevedel for his assistance with the maximum likelihood calculation.

During the second half of my Master's, I spent a lot of time in the Quantum Photonics Laboratory. I would like to acknowledge Rolf Horn, Evan Meyer-Scott, and Zhizhong Yan for out helpful discussions. Particular thanks to Chris Erven, with whom I have worked on the Sagnac source, and Hannes Hübel, who I partnered with to develop the photon triplet experiment.

On behalf of my colleagues and myself, I would like to acknowledge the agencies that have funded experiments on which I have worked. These are the Canadian Institute for Advanced Research, the Ontario Centres of Excellence, the Ontario Ministry of Research and Innovation, the Canadian Foundation for Innovation, and finally the National Science and Engineering Council of Canada, which also funded me personally during my Master's.

Finally, I would like to thank my parents Normand and Denise, my sister Elyse, and my girlfriend Catherine for their unconditional support.

Contents

List of Tables

List of Figures

Chapter 1

Theoretical background

1.1 Entanglement

Pure states

In the formalism of quantum mechanics, an isolated quantum system in a pure state is represented by a normalized vector $|\psi\rangle$, which belongs to a Hilbert space $\mathcal{H}$. Let us consider the case where we have a composite system made up of two subsystems [1], which we will call A and B. The state of the combined system is represented by a normalized vector on the Hilbert space $\mathcal{H}_{AB}$, which is defined as:

$$\mathcal{H}_{AB} = \mathcal{H}_A \otimes \mathcal{H}_B \tag{1.1}$$

where $\otimes$ represents the tensor product, and $\mathcal{H}_A$ and $\mathcal{H}_B$ are the Hilbert spaces corresponding to the two subsystems, called the factor spaces. For any pair of vectors $|\psi\rangle_A \in \mathcal{H}_A$ and $|\phi\rangle_B \in \mathcal{H}_B$, there is product vector $|\psi\rangle_A \otimes |\phi\rangle_B$ which is in $\mathcal{H}_{AB}$. The states represented by such product vectors are called *separable*. For these states, the whole system can be described by the state of its individual parts.

[1] We consider two subsystems for simplicity, but everything in this section can readily be generalized for any number of subsystems.

However, we know from the superposition principle that any normalized sum of state vectors is also a valid state vector. This is important because some of the states that can be constructed in this way are not separable. Any quantum state that is not separable is called *entangled*. This means that the state of the entire system can no longer be seen simply as a combination of the two states of the subsystems. Important examples include the Bell states:

$$\begin{aligned} |\phi^{\pm}\rangle &= \frac{1}{\sqrt{2}}|00\rangle \pm |11\rangle \\ |\psi^{\pm}\rangle &= \frac{1}{\sqrt{2}}|01\rangle \pm |10\rangle \end{aligned} \tag{1.2}$$

where $|0\rangle$ and $|1\rangle$ are the two basis states in the computational basis of a two level quantum system, commonly called a qubit. If only one of the qubits is measured, then the result is random. However, if both qubits are measured in the computational basis, the will be perfectly correlated for the $|\phi\rangle$ states and perfectly anti-correlated for the $|\psi\rangle$ states. Moreover, we can still observe perfect correlations in other bases. As an example, when the $|\psi^-\rangle$ state is written in any orthonormal basis $\{|\alpha\rangle, |\alpha_\perp\rangle\}$, it always has the form: $|\psi^-\rangle = \frac{1}{\sqrt{2}}(|\alpha\rangle|\alpha_\perp\rangle - |\alpha_\perp\rangle|\alpha\rangle)$. It is therefore easy to see that if the same measurement is performed on both qubits, the results will always be anti-correlated.

Mixed states

The definition of entanglement given above can be generalized for mixed (non-pure) states. In this case, the quantum state of a system is no longer represented by a state vector $|\psi\rangle$, but instead by a density matrix ρ, which is a Hermitian ($\rho^\dagger = \rho$), positive semi-definite operator, and has trace 1. A mixed state is said to be separable if it can be written as a convex sum of separable states:

$$\rho = \sum_i p_i \rho_i^A \otimes \rho_i^B. \tag{1.3}$$

If a state cannot be written in this way, then it is entangled.

Entanglement has been shown to exist in many different physical systems. In this work, we are specifically interested in the production of entangled *photons*. More precisely, we want to produce photons which are entangled in their polarization degree of freedom. We will therefore replace the basis vectors of the computational basis, $|0\rangle$ and $|1\rangle$, with the basis vectors $|H\rangle$ and $|V\rangle$ representing horizontal and vertical polarizations. In Section 1.3, we provide an explanation of the physical process most often used for the production of entangled photons: spontaneous parametric down-conversion. In Chapter 2, we will explain how this process can be used produce entangled systems of two and three photons.

Entangled photons can be seen as a resource for several applications. Two photon [1, 2, 3, 4, 5, 6, 7, 8, 9, 10, 11, 12] and multi-photon [13, 14, 15, 16] entanglement have been used extensively for fundamental tests of quantum mechanics. Entangled photons can also be utilized for quantum key distribution [17, 18, 19, 20], and are a resource for linear optics quantum computing [21], particularly cluster-state quantum computing [22, 23, 24, 25, 26].

.

1.2 Quantum state tomography

When we try to produce entangled photons, it is important to have a method to determine whether or not we succeeded. One (very thorough) way of doing this is to determine the entire quantum state of the photons. However, it is well known that it is impossible to completely measure the state of any single copy of a quantum system, because the system is disturbed by the measurement. This problem can be overcome if we have many copies of the same quantum system. It is then possible to reconstruct the density matrix corresponding to the quantum state of this system. The idea is to measure a number of observables, each one on a portion of the ensemble of quantum systems. This is called *quantum state tomography*.

In this section, we use a specific type of projective measurement where the system is only detected for a specific outcome of the measurement. Therefore, for a given measurement, our result corresponds to the number of detections recorded with the measurement device in a particular configuration. We call this number of detections *counts*.

1.2.1 Linear quantum state tomography

The minimum number of projective measurements required for quantum state tomography is directly related to the number of free parameters in the density matrix. Indeed, one projective measurement is required for every free parameter, with one extra measurement needed for normalization, since measurements determine quantities instead of probabilities. A system containing n qubits is represented by a 2^n by 2^n square density matrix, which has $4^n - 1$ free parameters. Hence, 4^n projective measurements are required for quantum state tomography of such a system [27].

Of course, the choice of these measurements is not arbitrary. In the case of a two qubit system, 16 measurements are needed. These measurements, consisting of projections onto the 16 vectors $|\psi_\nu\rangle$, are tomographically complete if and only if the 16x16 matrix with elements [2]:

$$B_{\nu,\mu} = \langle\psi_\nu|\hat{\Gamma}_\mu|\psi_\nu\rangle \tag{1.4}$$

is nonsingular. The $\hat{\Gamma}_\mu$ are the set of matrices $\hat{\sigma}_i \otimes \hat{\sigma}_j$, with $i, j = 0, 1, 2, 3$, where $\hat{\sigma}_0$ is the 2x2 identity, and the other $\hat{\sigma}_i$ are the Pauli matrices. The un-normalized reconstructed density matrix $\hat{\rho}$, is given by [27]

$$\hat{\rho} = \sum_{\nu=1}^{16} \left[\sum_{\mu=1}^{16} (B^{-1})_{\nu,\mu} \hat{\Gamma}_\mu \right] n_\nu \tag{1.5}$$

where n_ν is the number of counts for the $|\psi_\nu\rangle$ measurement. This method thus provides a simple way of calculating an estimate of a quantum state given the appropriate measurements. There are some shortcomings however. First, it does not allow us to take into account any additional measurements. For example, for a two qubit system linear quantum state tomography requires exactly 16 measurements. If we have a set of more than 16 measurements, also called a tomographically over-complete set of measurements, some of them will have to be excluded. Second, the density matrices calculated with this method can be un-physical, especially when the states are very pure. These limitations are addressed by another procedure used to reconstruct quantum states, called *maximum likelihood*.

[2] in this section, we use the ˆ to identify matrices, not only quantum mechanical operators.

1.2.2 Maximum likelihood quantum state tomography

The idea of the maximum likelihood method is to use the same measurements as in Section 1.2.1 to reconstruct a state, but with the added constraint that the reconstructed density matrix must be physical. To do this, we start by writing parameterizing the density matrix, $\hat{\rho}$, as:

$$\hat{\rho} = \frac{\hat{T}^\dagger \hat{T}}{\mathrm{Tr}\left[\hat{T}^\dagger \hat{T}\right]} \tag{1.6}$$

where the † indicates the Hermitian conjugate, and $\hat{T}$ is a square matrix of dimension d. Writing $\hat{\rho}$ as proportional to $\hat{T}^\dagger \hat{T}$ ensures that it is hermitian and positive. Dividing by $\mathrm{Tr}\left[\hat{T}^\dagger \hat{T}\right]$ ensures that it is normalized. The matrix $\hat{T}$ could have up to $2d^2$ parameters, but we know that $\hat{\rho}$ only has $d^2 - 1$ free parameters. We thus need to write $\hat{T}$ without any unneeded parameters, but in such a way that the entire space of density matrices is available for $\hat{\rho}$ [28]. This can be done by writing $\hat{T}$ as a triangular matrix, with real numbers on the diagonal [27]. For a two qubit system, this would be written as:

$$T = \begin{pmatrix} t_1 & 0 & 0 & 0 \\ t_5 + it_6 & t_2 & 0 & 0 \\ t_{11} + it_{12} & t_7 + it_8 & t_3 & 0 \\ t_{15} + it_{16} & t_{13} + it_{14} & t_9 + it_{10} & t_4 \end{pmatrix}$$

which gives 16 free parameters.

The next step is to provide a measure of how well a given reconstruction of the density matrix agrees with the measurement results. To do this, we first consider that for a given reconstructed density matrix $\hat{\rho}$, we can predict the average number of counts for a measurement. This is given by:

$$\bar{n}_\nu = N\langle\psi_\nu|\hat{\rho}|\psi_\nu\rangle \tag{1.7}$$

where N is a constant related to the flux and detector efficiency. We then assume that the probability of obtaining n_ν can be approximated by a Gaussian distribution centered around $\bar{n}_\nu$. Therefore the probability that a given set of κ counts $\{n_\nu\}$ are measured is given by:

$$P\{n_1, n_2, ...n_\kappa\} = \frac{1}{N_{norm}} \prod_{\nu=1}^{\kappa} \exp\left[-\frac{(\bar{n}_\nu - n_\nu)^2}{2\bar{n}_\nu}\right] \tag{1.8}$$

where N_{norm} is a normalization constant. By combining Equations 1.7 and 1.8, we obtain:

$$P\{n_1, n_2, ...n_\kappa\} = \frac{1}{N_{norm}} \prod_{\nu=1}^{\kappa} \exp\left[-\frac{(N\langle\psi_\nu|\hat{\rho}|\psi_\nu\rangle - n_\nu)^2}{2N\langle\psi_\nu|\hat{\rho}|\psi_\nu\rangle}\right] \tag{1.9}$$

where the state $\hat{\rho}$ would be written as a function of the parameters t_i. The best state is the one for which the number of counts measured $\{n_1, n_2, ...n_\kappa\}$ is the most probable. Finding the best state then reduces to maximizing this function over the parameters t_i. In practice, instead of maximizing this function, we maximize its logarithm. So the mathematical problem becomes a minimization over the $d^2 - 1$ parameters t_i of the following function:

$$L\{t_1, t_2, ...t_{d_2-1}\} = \sum_{\nu=1}^{\kappa} \left[\frac{(N\langle\psi_\nu|\rho|\psi_\nu\rangle - n_\nu)^2}{2N\langle\psi_\nu|\rho|\psi_\nu\rangle}\right]. \tag{1.10}$$

As we have already mentioned, the first advantage of this method is that the resulting density matrix will always be physical. We are, in a way, using some additional information that we know about the matrix (the fact that it represents a physical system) to help with the reconstruction. The other major advantage of this technique is that it works with an arbitrarily large number of measurements. Indeed, κ can be larger than $d^2 - 1$. This means that we can use a tomographically over-complete set of measurements to get a better estimate of the state. We will use the maximum likelihood method to reconstruct the states produced in Chapter 3.

1.3 Spontaneous parametric down-conversion

The most commonly used method for producing entangled photon pairs, and the method which is used throughout the work described in this thesis, is spontaneous parametric down-conversion (SPDC). It can roughly be explained as the splitting of a "pump" photon into two photons of lesser energies, the "signal" and the "idler". SPDC is a strictly quantum effect; it cannot be explained in terms of classical nonlinear optics.

The usual way to treat SPDC is to start with its Hamiltonian. It can be derived by starting with the classical electric field energy density for a nonlinear medium, and then quantizing the electric field [29]. The resulting Hamiltonian is [30]:

$$\hat{H} = \epsilon_0 \int_V d^3r \chi^{(2)} \hat{E}_p^{(+)} \hat{E}_s^{(-)} \hat{E}_i^{(-)} + H.c. \tag{1.11}$$

where ϵ_0 is the vacuum permittivity, $H.c.$ is the Hermitian conjugate and s and i are indices representing the two down-converted modes, the signal and idler. The integral is over the volume V, which is the volume of the nonlinear crystal which is illuminated by the pump beam. In this equation, it is assumed that only one element of the nonlinear susceptibility tensor $\chi^{(2)}$ must be considered. We assume that the pump field is intense and negligibly depleted, so that it can be treated classically as a monochromatic wave. We thus write it as:

$$\hat{E}_p^{(+)} = E_0 e^{i(\vec{k_p}\cdot\vec{r} - \omega_p t)}. \tag{1.12}$$

We cannot do the same for the signal and idler fields, $\hat{E}_s^{(-)}$ and $\hat{E}_i^{(-)}$, which we must keep quantized as they describe single photon level fields. We can write them as:

$$\hat{E}_j^{(-)} = -i \sum_k \sqrt{\frac{\hbar\omega_{k,j}}{2\epsilon_0 V}} \vec{\epsilon}_k \hat{a}_{k,j}^\dagger e^{-i(\vec{k_j}\cdot\vec{r} - \omega_{k,j} t)} \tag{1.13}$$

where $j = s, i$ to represent either the signal or the idler, $\hat{a}^\dagger$ is the creation operator, $\vec{\epsilon}_k$ is a unit polarization vector. This equation is a bit more general than what we need for

our purposes, and so we will make a few assumptions. For more general treatments, see [29, 31, 32, 33]. We will first assume that all the fields are plane waves traveling in the z direction. Equation 1.12 thus becomes:

$$E_p^{(+)} = E_0 e^{i(k_p z - \omega_p t)} \tag{1.14}$$

and Equation 1.13 is simplified to:

$$\hat{E}_j^{(-)} = -i \sum_k \sqrt{\frac{\hbar \omega_{k,j}}{2\epsilon_0 V}} \hat{a}_{k,j}^\dagger e^{-i(k_j z - \omega_{k,j} t)} \tag{1.15}$$

We also only look at a single mode from the signal and idler fields. We can therefore drop the sum over k. So we have:

$$\hat{E}_j^{(-)} = -i \sqrt{\frac{\hbar \omega_j}{2\epsilon_0 V}} \hat{a}_j^\dagger e^{-i(k_j z - \omega_j t)}. \tag{1.16}$$

Let us now look at the quantum state produced by this Hamiltonian. We assume that the quantum field is initially in the vacuum state. The quantum state's evolution is given by:

$$|\psi(t)\rangle = \exp\left[\frac{1}{i\hbar} \int_0^t dt' \hat{H}(t')\right] |\text{vac}\rangle \tag{1.17}$$

where $|\text{vac}\rangle$ represents the vacuum state. We expand the exponential to the first order, which gives us:

$$|\psi(t)\rangle = |\text{vac}\rangle + \frac{1}{i\hbar} \int_0^t dt' \hat{H}(t') |\text{vac}\rangle. \tag{1.18}$$

Now by combining Equations 1.11, 1.14, 1.16 and 1.18, and only considering the non-vacuum portion, we obtain:

$$|\psi(t)\rangle \sim \frac{1}{i\hbar}\epsilon_0 E_0 \int_0^t dt' \int_V d^3r \chi^{(2)} \left[-i\sqrt{\frac{\hbar\omega_s}{2\epsilon_0 V}}\right]\left[-i\sqrt{\frac{\hbar\omega_i}{2\epsilon_0 V}}\right] \hat{a}_s^\dagger \hat{a}_i^\dagger e^{i(k_p-k_s-k_i)z} e^{i(\omega_s+\omega_i-\omega_p)t}|\text{vac}\rangle. \tag{1.19}$$

Note that the Hermitian conjugate portion of the Hamiltonian is gone, as it contains lowering operators acting on the vacuum. Because we assumed plane waves, we can easily do the integration over x and y. This, and a few simplifications, gives us:

$$|\psi(t)\rangle \sim \frac{iE_0 L_x L_y \sqrt{\omega_s\omega_i}}{2V} \int_0^t dt' e^{i(\omega_s+\omega_i-\omega_p)t} \int_0^{L_z} dz \chi^{(2)} e^{i(k_p-k_s-k_i)z}|1\rangle_s|1\rangle_i \tag{1.20}$$

where L_x and L_y are the height and width of the crystal. For now, we take $\chi^{(2)}$ to have no z dependance (in contrast to what we will do in Section 1.4), and we can do both integrations. We find:

$$|\psi(t)\rangle \sim \frac{iE_0 L_x L_y \sqrt{\omega_s\omega_i}}{2V} \chi^{(2)} e^{i\frac{\Delta\omega}{2}t} t \,\text{sinc}\left(\frac{\Delta\omega t}{2}\right) e^{i\frac{\Delta k}{2}L_z} L_z \,\text{sinc}\left(\frac{\Delta k L_z}{2}\right)|1\rangle_s|1\rangle_i \tag{1.21}$$

where $\Delta\omega = \omega_s + \omega_i - \omega_p$ and $\Delta k = k_p - k_s - k_i$. The interaction time, t, is long enough that the first sinc function can be approximated as a delta function [31], so that we have:

$$|\psi(t)\rangle \sim \frac{iE_0 \sqrt{\omega_s\omega_i}}{2} \chi^{(2)} e^{i\frac{\Delta\omega}{2}t} e^{i\frac{\Delta k}{2}L_z} \delta\left(\frac{\Delta\omega}{2}\right) \text{sinc}\left(\frac{\Delta k L_z}{2}\right)|1\rangle_s|1\rangle_i. \tag{1.22}$$

We can observe that this result shows that the signal and photons are only produced in pairs. Also, we notice that because of the delta function, we can only have pairs if the following condition is met:

$$\omega_p = \omega_s + \omega_i. \tag{1.23}$$

This essentially means that the energies of the two created photons equal the energy of one pump photon. This is why down-conversion is sometimes called "photon splitting". We will also observe the because of the sinc $\left(\frac{\Delta k L_z}{2}\right)$ term, the signal will be maximal when:

$$k_p = k_s + k_i. \tag{1.24}$$

This relation is called phasematching. It is related to the fact that the pump beam must stay in phase with the signal and idler beams in order for the signal power to constructively interfere throughout the crystal.

Let us finally note for completeness that there are different types of SPDC, based on the polarization of the pump, signal and idler. Different conventions exist, but in this work we will use the convention that there are two types of SPDC. An SPDC process is of type I if both signal and idler have the same polarization. It is of type II if the signal and idler have perpendicular polarizations.

1.4 Quasi-phasematching

In the previous section, we saw that for SPDC to happen, we need the phase mismatch Δk to approach zero. How can we do this? It is in fact not trivial, as the dispersion in materials generally causes Equation 1.24 to not be satisfied. Therefore, we need to modify the material, in order to change the effective indices of refraction for the pump, signal and idler, so that $\Delta k = 0$. The first methods that have been used to do this are temperature tuning and angle tuning. Both of these methods make use of the birefringence of the materials in order to compensate for the dispersion[34]. However, these methods have several important limitations:

- Some materials with high optical nonlinearities are not birefringent, or have insufficient birefringence, particularly at shorter wavelengths.
- Some of the nonlinear coefficients are not affected by birefringence. For example, the d_{33} element of the contracted nonlinear susceptibility tensor[3] is much larger than others for many materials, but it is only relevant when all three waves are polarized along the same direction.

[3]The contracted nonlinear susceptibility tensor is a notation used in materials with Kleinman symmetry. It is proportional to $\chi^{(2)}$. For example, $d_{33} = \frac{1}{2}\chi^{(2)}_{zzz}$. For more details, see section 1.5.6 of [34].

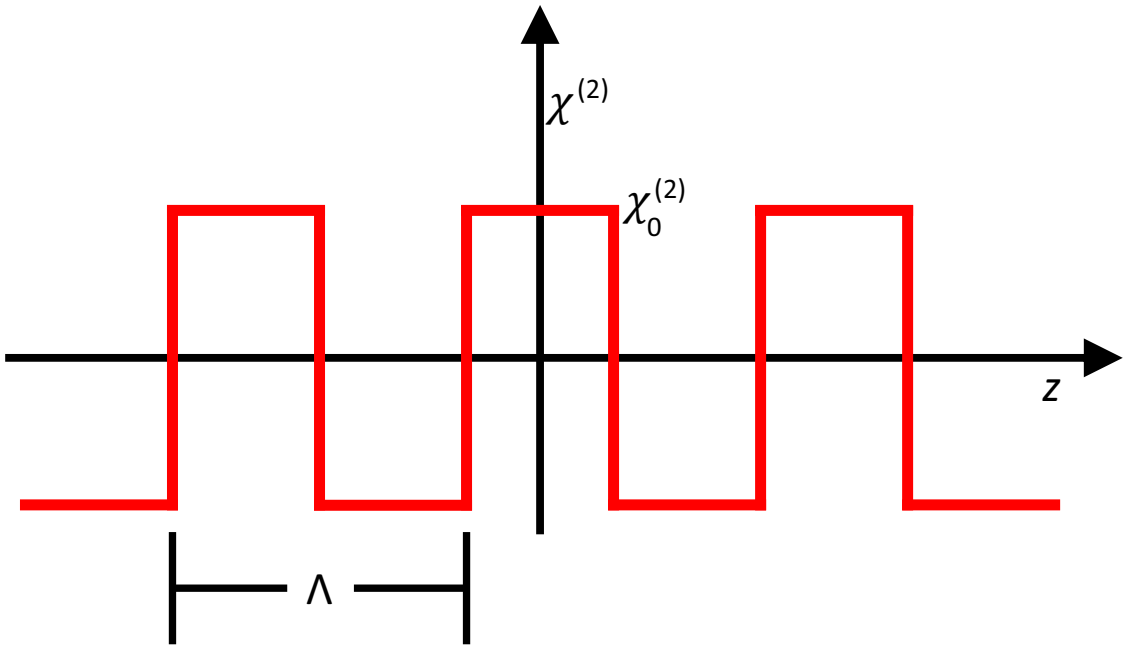

Figure 1.1: Effective nonlinear coefficient in a periodic material. The nonlinear coefficient can be written as a step function, which goes from $\chi_0^{(2)}$ to $-\chi_0^{(2)}$, with a period of Λ.

- Because the direction of propagation in the crystal is dictated by the phasematching, it is usually not along one of the crystallographic axes. This leads to spatial walk-off, which limits the length of crystals that can be used.

This is where quasi-phasematching comes in. It is often seen as an alternative to angle or temperature tuning, although it was actually proposed *before* these methods by Armstrong et al. in 1962 [35]. A good review of the subject can be found in [36]. Here we will go through the basic theory of quasi-phasematching. Periodically reversing the nonlinear medium leads to an effective nonlinear coefficient $\chi^{(2)}$ like the one shown in Figure 1.1. This can be written as:

$$\chi^{(2)}(z) = \chi_0^{(2)} \operatorname{sgn}\left(\cos\frac{2\pi z}{\Lambda}\right) \tag{1.25}$$

where $\chi_0^{(2)}$ is the nonlinear coefficient of the material, z represents the position within the material, and sgn is the sign function, which returns 1 for positive arguments and -1 for negative arguments. We can write $\chi^{(2)}(z)$ as a Fourier series:

$$\chi^{(2)} = \sum_{m=-\infty}^{\infty} G_m e^{ik_m z} \tag{1.26}$$

where $k_m = \frac{2\pi m}{\Lambda}$. The coefficients G_m are given by:

$$G_m = \frac{1}{\Lambda} \int_{-\Lambda/2}^{\Lambda/2} \chi^{(2)} e^{-ik_m z}\, dz. \tag{1.27}$$

Using the fact that $\chi^{(2)}$ is an even function, the integral is easily evaluated, and we find:

$$G_m = \frac{2\chi_0^{(2)}}{\pi m} \sin\Big(\frac{m\pi}{2}\Big). \tag{1.28}$$

We can substitute this back into 1.25, and get:

$$\chi^{(2)} = \sum_{m=-\infty}^{\infty} \frac{2\chi_0^{(2)}}{\pi m} \sin\Big(\frac{m\pi}{2}\Big) e^{i\frac{2\pi m}{\Lambda} z}. \tag{1.29}$$

We could insert this directly into Equation 1.20. We would then get a summation of integrals, one for each term of the Fourier series. However, we only need one of these terms to be large in order to get signal. In other words, we only need one of the terms to fit the phasematching conditions. Because the coefficients of the Fourier series get smaller as $|m|$ grows, we will choose to keep only the $m = -1$ term[4]. We thus have:

$$\chi^{(2)} = \frac{2\chi_0^{(2)}}{\pi} e^{-i\frac{2\pi}{\Lambda} z} \tag{1.30}$$

[4]We could just as well have chosen $m = 1$. This would simply change the sign of the $\frac{2\pi}{\Lambda}$ term in Equation 1.32. In practice, the sign is chosen such that Equation 1.32 can be solved.

If we now substitute this into equation Equation 1.20, we get :

$$|\psi(t)\rangle \sim \frac{iE_0L_xL_y\sqrt{\omega_s\omega_i}}{\pi V}\int_0^t dt' e^{i(\omega_s+\omega_i-\omega_p)t}\int_0^{L_z} dz\chi_0^{(2)}e^{i(k_p-k_s-k_i-\frac{2\pi}{\Lambda})z}|1\rangle_s|1\rangle_i \tag{1.31}$$

We can then integrate this equation like we did for Equation 1.20. The only difference compared to perfect phasematching, other than the factor of $2/\pi$, is that because there is an extra term in the exponential in z, the phasematching condition changes. Instead of $\Delta k = k_p - k_s - k_i$, we have $\Delta k = k_p - k_s - k_i - \frac{2\pi}{\Lambda}$. Since we still need $\Delta k \approx 0$, we have the quasi-phasematching condition:

$$k_p = k_s + k_i + \frac{2\pi}{\Lambda}. \tag{1.32}$$

This new phasematching condition now depends on the period Λ, so we have a new parameter at our disposal that we can choose freely in order to satisfy the phasematching condition. Therefore, we do not need to use angle tuning. This leads to two distinct advantages. First, we can chose the period Λ so that collinear down-conversion is phasematched. This makes it much easier to collect all of the signal and idler photons produced. The second advantage is that we can now choose to have the beams traveling along one of the crystal's crystallographic axes. This then eliminates the problems caused by spatial walk-off, and therefore allows us to use much longer crystals, which again leads to an increased signal.

1.5 Periodic poling

In the previous section, a very important detail was omitted. We simply assumed that we could periodically reverse the sign of the nonlinear coefficient, without explaining how this can actually be done. In their 1962 paper, Armstrong et al. suggested cutting a nonlinear crystal into thin slices, and then to reassemble it, rotating every second slice by 180°. In theory this would work, except that by using real parameters in Equation 1.32, one finds that Λ has to be of the order of $1 - 100\mu$m. This makes this method impractical.

Instead, the most common method now used to fabricate nonlinear crystals for quasi-phasematching is *periodic poling*. This method, first demonstrated by Yamada et al. [37], works for ferroelectric materials. The idea, shown in Figure 1.2, is to apply electrodes on a crystal, once every period. By applying a voltage to these electrodes, an electric field is created in the material. This electric field inverts the orientation of the domains in the material, thus inverting the sign of $\chi^{(2)}$. This method has been applied to many ferroelectric materials. Most fall into two categories :

- The lithium niobate ($LiNbPO_3$ or LN) and lithium tantalate ($LiTaO_3$ or LT) family. Lithium niobate has the largest nonlinear coefficient of the commonly used ferroelectrics (d_{33} = 28pm/V). Periods as small as 1.4μm can be fabricated. These materials are most commonly used in the near infrared, but wavelengths of between 460nm to 2.8μm have been reached using difference or sum frequency generation.[36]

- Potassium tytanyl phosphate ($KTiPO_4$ or KTP) and its isomorphs, ($RbTiPO_4$ and $KTiAsO_4$). These have smaller nonlinear coefficients (d_{33} = 15pm/V - 17pm/V), but have higher damage thresholds. Uniform polling periods of $4 - 39\mu m$ can be obtained in crystals as long as 30mm. KTP is usually used in the visible to near UV region of the spectrum. Wavelengths as low as 359nm have been reached using second harmonic generation in periodically poled KTP[36]. This implies that it can be used for SPDC with a pump wavelength as low as 359nm.

In general, periodic polling is not precise enough to achieve the exact period needed for phasematching. Fine adjustment of the phasematching is usually done using temperature tuning. In the case of down-conversion, we can chose the wavelength of the signal and idler by changing the crystal temperature. The experimental observation of this effect is shown for PPKTP in Section 3.4.1, and the theoretical predictions can be found in Appendix B. For PPLN, the effect is shown in Figure 4.3.

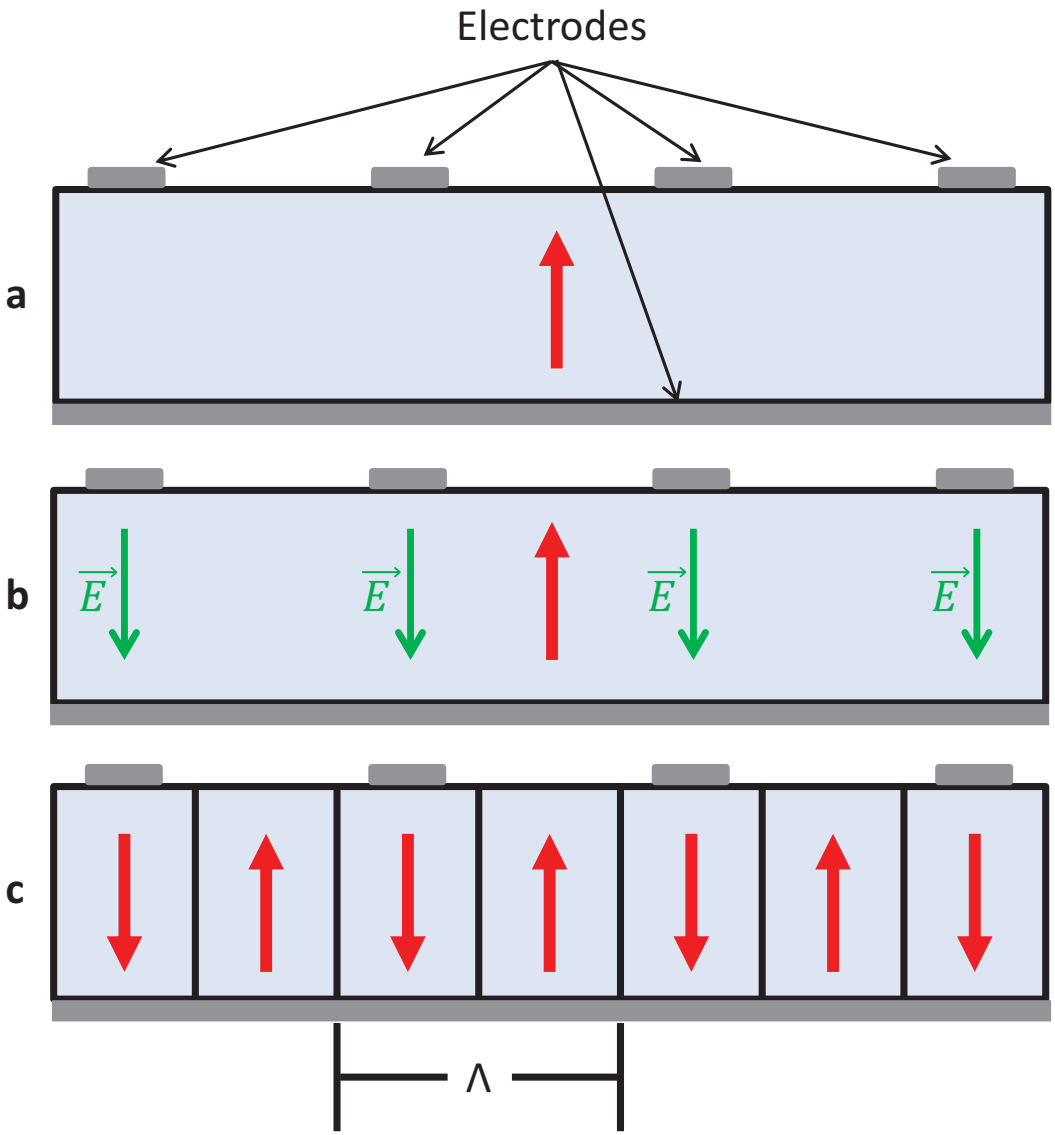

Figure 1.2: Sketch of the periodic poling method. **a**, In the beginning, all the domains point in the same direction indicated by the red arrow. **b**, An electric field is then applied in the opposite direction, inverting the domains in the affected regions. **c**, We are left with the desired periodic material.

Chapter 2

Polarization entangled photons from SPDC

2.1 Using SPDC to get polarization entangled photon pairs

In this section, we will give a brief review of the different methods that have been used to produce photon pairs entangled in polarization. Helpful references on the subject, which we used for this section, are [38] and [39].

2.1.1 The first entangled photons from SPDC

Polarization entangled photons produced with SPDC were first demonstrated in [5, 6]. This method, shown in Figure 2.1, uses a type I SPDC process. The polarization of one of the photons is rotated by 90°. The two photons are then brought back together on a $50:50$ beam splitter to interfere. The resulting state is:

$$|\psi\rangle = \frac{1}{\sqrt{2}}\left(|H\rangle_a + i|H\rangle_b\right) \otimes \left(-i|V\rangle_a + |V\rangle_b\right) \tag{2.1}$$

$$= \frac{1}{2}\left(|H\rangle_a|V\rangle_b + |V\rangle_a|H\rangle_b - i|H\rangle_a|V\rangle_a + i|V\rangle_b|H\rangle_b\right), \tag{2.2}$$

which is a state that is not entangled. However, if we choose to only consider the cases when a photon is detected in both modes a and b at the same time, then the produced state is:

$$|\psi\rangle = \frac{1}{\sqrt{2}}\left(|H\rangle_a|V\rangle_b + |V\rangle_a|H\rangle_b\right) \tag{2.3}$$

which is a maximally entangled Bell state. This method uses so-called *post-selection*[1]. From the full quantum state which is produced in Equation 2.2, only certain parts are chosen to obtain the desired quantum state of Equation 2.3. The procedure is probabilistic, only working half of the time in this case. Even if all the photons could be detected, only half of them would belong to the entangled state 2.2. This method is therefore not appropriate for certain fundamental tests of quantum mechanics, such as a loophole free Bell's inequality experiment [40], or for linear optics quantum computing[21]. Let us also note that the technique can be adapted to use type II SPDC [41].

2.1.2 Type II SPDC single emitter scheme

In 1995, Kwiat et al. [8] demonstrated the first *direct* source of entangled photons using SPDC, i.e. a source without the need for post-selection (of the kind described in Footnote 1). This scheme is illustrated in Figure 2.2. The phasematching conditions are chosen so

[1]In practice, we always use some kind of post-selection to produce entangled photons. This is in part due to the probabilistic nature of SPDC (because we don't know when pairs of photons will be produced) and to the limited efficiency of coupling and detectors (when one photon is detected, its partner might have been lost). So, in practice, we always only consider simultaneous detections, and this is a form of post-selection. The post-selection needed for the scheme in Section 2.1.1 is different; even if SPDC was deterministic and if we had perfect detectors, it would still be required. In the rest of this thesis, we will use the term post-selection to refer specifically to this specific kind of "essential" post-selection.

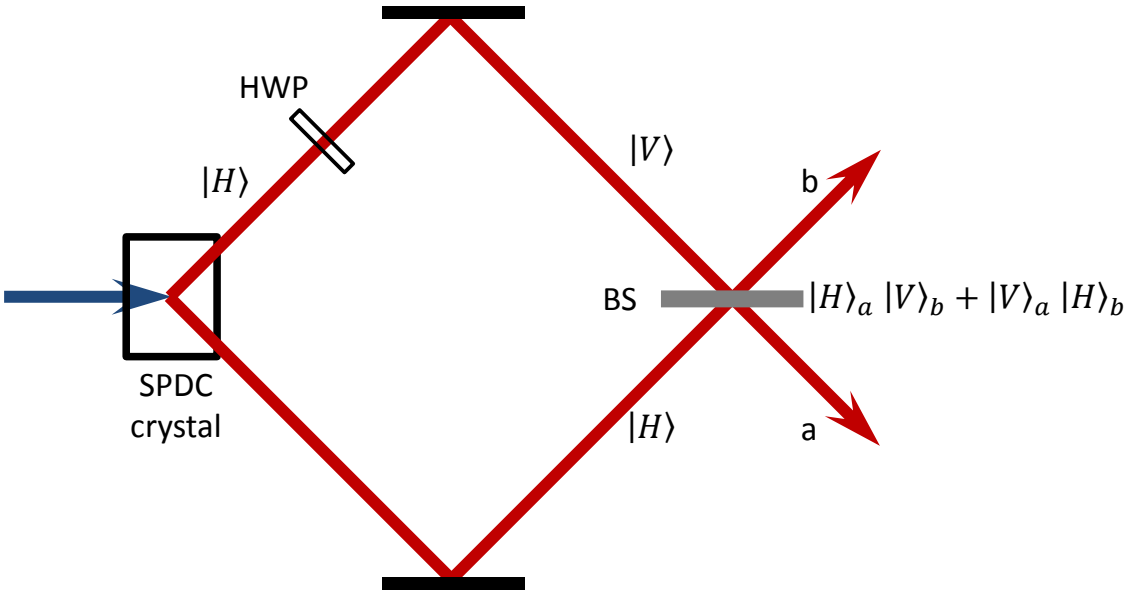

Figure 2.1: The first successful method for the generation of polarization entangled photons using SPDC. A pump produces type I down-conversion in a nonlinear medium. The polarization of one of the pairs is flipped using a half-wave plate (HWP). The pairs are then recombined on a 50 : 50 beam splitter (BS). The labels a and b indicate the two output modes of the BS.

that the two conical surfaces along which the signal and idler photons are emitted intersect along the lines a and b. If a signal photon is emitted in direction a, then an idler is emitted in direction b, and vice-versa. This ensures that the state produced satisfies:

$$|\psi\rangle = \frac{1}{\sqrt{2}}\left(|H\rangle_a|V\rangle_b + e^{i\phi}|V\rangle_a|H\rangle_b\right) \tag{2.4}$$

The phase ϕ is set by placing a birefringent material in one of the optical paths after the crystal. This method is not probabilistic in the same way as the scheme described in Section 2.1.1. Indeed, here if one was able to detect all of the photons emitted along the directions a and b, every one of them would belong to an entangled pair. The other advantage of this scheme is that entangled photons are produced along two distinct spatial modes, which can readily be collected into single mode fibres. Its downside is that by only using the photons from the intersection of the cones, a majority of the photons produced by SPDC are lost. Also note that because of birefringence in the nonlinear crystal, the signal and idler suffer from both longitudinal and transverse walk-off. This walk-off can be compensated by placing a nonlinear crystal, half the length of the down-converter but identical otherwise, in each of the output modes.

2.1.3 Type I SPDC sandwich scheme

Another source of entangled photon using SPDC was presented by Kwiat et al. in 1999 [42]. It is shown in Figure 2.3. This method uses two identical emitters, but one of them is rotated by 90°. With the pump polarized at 45°, pairs may be produced either in the first crystal ($|HH\rangle$) or in the second crystal ($|VV\rangle$). As long as there is no information left which would allow one to infer from which crystal a photon originated, then the resulting quantum state is the entangled state:

$$|\psi\rangle = \frac{1}{\sqrt{2}}\left(|H\rangle_a|H\rangle_b + e^{i\phi}|V\rangle_a|V\rangle_b\right) \tag{2.5}$$

where the phase ϕ can be chosen by changing the input polarization. The advantage of this method over the single emitter type I scheme is that a much larger proportion of the

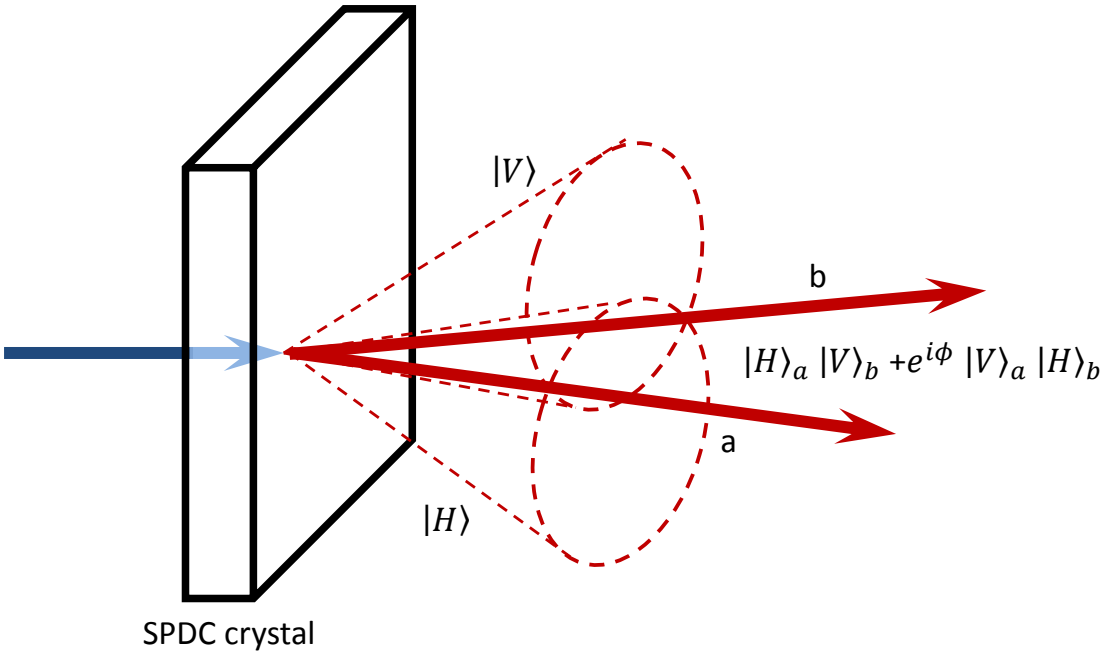

Figure 2.2: Type II SPDC single emitter source of entangled photons. The signal and idler photons are each emitted along a conical surface. By collecting photons from the intersection of these surfaces (a and b), a maximally entangled state can be obtained.

produced photons are entangled. However, in order to have indistinguishability in this configuration, the crystals need to be thin, thus limiting the brightness of this kind of source. Just like for the single type-II single emitter scheme, compensation crystals are needed to compensate for the the transverse and longitudinal walk-off of the signal and idler. Furthermore, if a pulsed pump is used, then additional compensation is needed to compensate the longitudinal walk-off between the horizontal and vertical components of the pump beam [43].

A variation of the sandwich source is to use collinear and non-degenerate SPDC[44]. In this case, the signal and idler do not have the same wavelength, and can be split up using a dichroic mirror. This method is advantageous as almost all of the photons from the SPDC are collected, and much longer crystals may be used. Its disadvantage is that the scheme does not work when the signal and idler need to have the same wavelength.

2.1.4 Interferometric SPDC schemes

One way of using degenerate and collinear SPDC is to place two down-converters inside an interferometer, as shown in Figure 2.4. In this scheme, two type II down-converters are placed inside a Mach-Zehnder interferometer. They both produce $|HV\rangle$ pairs, which are then recombined on a polarizing beam splitter (PBS). The resulting state is:

$$|\psi\rangle = \frac{1}{\sqrt{2}}\left(|H\rangle_a|V\rangle_b + e^{i\phi}|V\rangle_a|H\rangle_b\right) \tag{2.6}$$

The phase ϕ is again controlled by changing the input polarization. The advantage of this method is that it allows for collinear SPDC, which equates to longer crystals and to more photons being collected. The disadvantage is that it requires the interferometer to be phase-stable, and thus usually requires sophisticated stabilization. The method was proposed by [40]. The first demonstration of an interferometric SPDC scheme was reported in [45], although in this case, a type I SPDC source was used, so there were not two separate output modes as in Figure 2.4, which is one of the main benefits of this technique. The first demonstration with a type II source was done in [46]. This setup was further improved using a folded interferometer in [47], but the quality of the entanglement was still limited

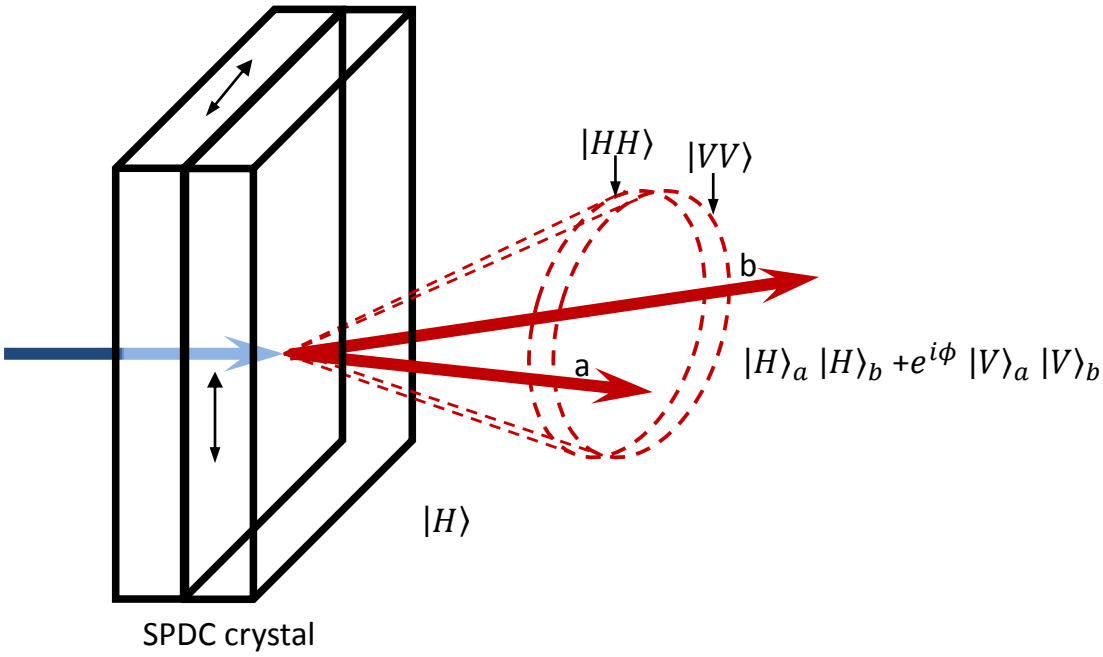

Figure 2.3: Type I SPDC sandwich configuration source of entangled photons. Two type I emitters are "sandwiched" together , with the second one rotated by 90°. The first emitter can produce $|HH\rangle$ pairs, and the second $|VV\rangle$ pairs. If there is no way of distinguishing from which crystal the photons come, then the produced state is maximally entangled.

by the phase stability of the interferometer. In Chapter 3, we describe an entangled photon source which gets around this problem by using an inherently phase-stable Sagnac interferometer.

2.2 Using SPDC to produce polarization entangled photon triplets

In this section, we describe methods that have been used to produce three photon entanglement using SPDC. Three photon entanglement is different than the in two photon case, because there exist two different classes of entangled states: the Greenberger-Horne-Zeilinger (GHZ) class of states and the W class of states [48, 49]. We have included a short review of the different methods that have been used to produce GHZ states, and we give an example of how W states can be produced.

2.2.1 GHZ states

GHZ state with double pairs from a single emitter

The first demonstration of a three photon GHZ state was done by Bouwmeester at al. [50]. Their scheme is shown in Figure 2.5. The production of a GHZ state with this setup can be understood as follows: the SPDC source is pumped by a pulsed laser, and set up to produce entangled pairs in the state of the form: $|\psi\rangle = \frac{1}{\sqrt{2}}(|H\rangle_{\rm a}|V\rangle_{\rm b} - |V\rangle_{\rm a}|H\rangle_{\rm b})$, using the single emitter scheme described in Section 2.1.2. We consider the case where two photon pairs are produced by the same pulse. To treat this appropriately, we need to look at the next term of the expansion in Equation 1.18, with two type II down-converters. The bandwidth of the pump and the filtering of the down-conversion are such that a simple single mode model suffices. Neglecting phasematching considerations, we can write the double-pair contribution to the quantum state in modes a and b as proportional to:

$$|\psi\rangle \sim \left(\hat{a}^{\dagger}_{H,{\rm a}}\hat{a}^{\dagger}_{V,{\rm b}} + \hat{a}^{\dagger}_{V,{\rm a}}\hat{a}^{\dagger}_{H,{\rm b}}\right)^2 |vac\rangle. \tag{2.7}$$

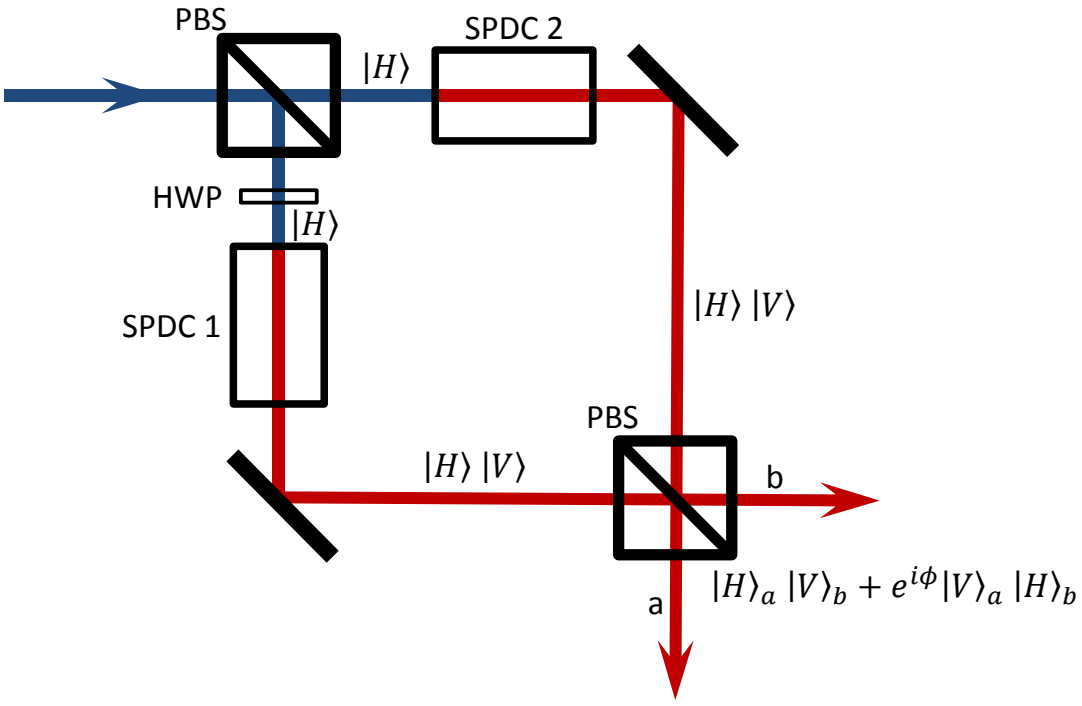

Figure 2.4: Interferometric source of entangled photons. Two type II down-converters are placed in each arm of a Mach-Zehnder interferometer. The vertical portion of the pump which is reflected by the PBS is rotated to horizontal with a half-wave plate (HWP). Depending on which down-converter a pair came from, the output is either $|H\rangle_a|V\rangle_b$ or $|V\rangle_a|H\rangle_b$. If the interferometer is stable, then the produced state is a coherent superposition of these two cases.

where the subscripts H and V indicate the polarization of created photons, and a and b the mode they are emitted in. If we expand this and let the operators act on the vacuum state, we get:

$$|\psi\rangle \sim 2\left(|2\rangle_{H,\mathrm{a}}|2\rangle_{V,\mathrm{b}} + |1\rangle_{H,\mathrm{a}}|1\rangle_{V,\mathrm{b}}|1\rangle_{V,\mathrm{a}}|1\rangle_{H,\mathrm{b}} + |2\rangle_{V,\mathrm{a}}|2\rangle_{H,\mathrm{b}}\right). \tag{2.8}$$

Here, the label in the brackets indicates the number of photons of a given polarization in a mode. The individual terms in this equation will be transformed in the setup as follows:

$$|H\rangle_{\mathrm{a}} \rightarrow |H\rangle_T \tag{2.9}$$

$$|V\rangle_{\mathrm{b}} \rightarrow \frac{1}{\sqrt{2}}\left(|V\rangle_2 + |V\rangle_3\right) \tag{2.10}$$

$$|V\rangle_{\mathrm{a}} \rightarrow \frac{1}{\sqrt{2}}\left(|V\rangle_1 + |H\rangle_2\right) \tag{2.11}$$

$$|H\rangle_{\mathrm{b}} \rightarrow \frac{1}{\sqrt{2}}\left(|H\rangle_1 + |H\rangle_3\right). \tag{2.12}$$

We can substitute these into Equation 2.8. We then expand this term, and we *post-select* only the terms where there is a photon in each of the four output modes. With appropriate renormalization, we find:

$$|\psi\rangle = \frac{1}{\sqrt{2}}|H\rangle_T\left(|V\rangle_1|V\rangle_2|H\rangle_3 + |H\rangle_1|H\rangle_2|V\rangle_3\right). \tag{2.13}$$

which is a GHZ state when the trigger term is traced out. There is a resemblance between this method for producing GHZ states and the method described in Section 2.1.1 to produce Bell pairs. This is because in both cases, post-selection is critical to observing the entangled state. Even with perfect detectors, most of the photons detected in any of the output modes would not belong to a GHZ state. Indeed, there is only a 1/8 probability that all the photons go to different detectors.

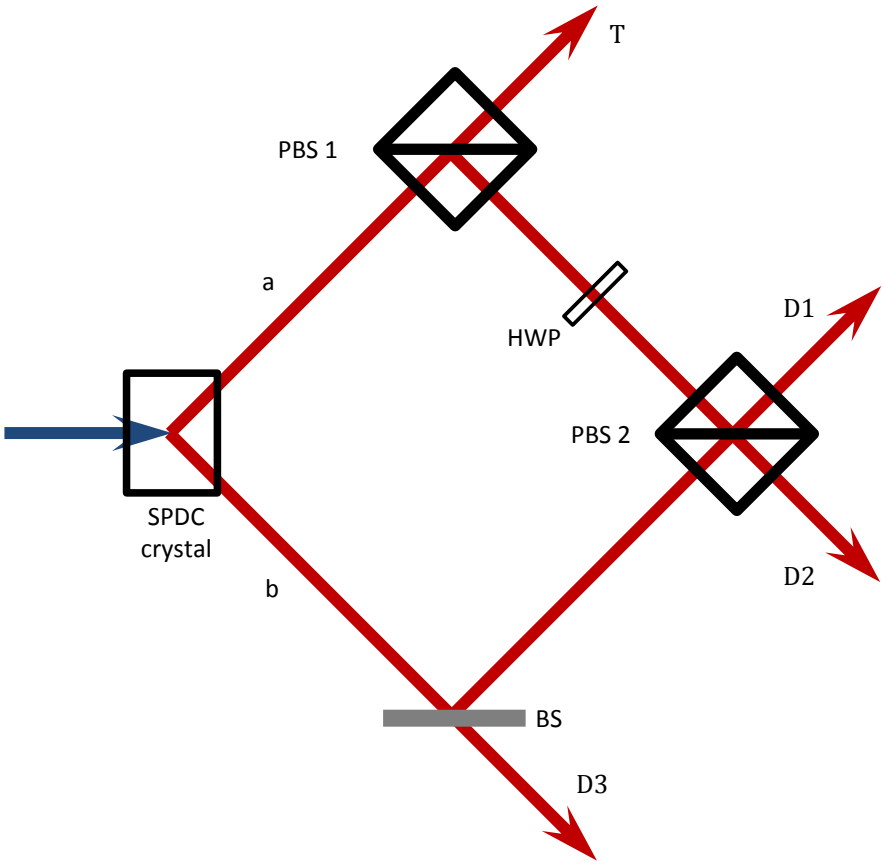

Figure 2.5: Double pairs from a single emitter setup used for the first production of GHZ states. An SPDC source is pumped with a pulsed laser to produce entangled pairs. Detectors are placed in each of the output modes T, D1, D2 and D3. In the case where two pairs are produced at the same time, and by post-selecting on the cases where all four detectors get a detection, a GHZ state is produced.

GHZ state by interfering two independent sources

Another method which can be used to produce GHZ states was implemented for the first time in [51] and is shown in Figure 2.6. Here, two nonlinear crystals are pumped by a pulsed laser. They are configured to produce entangled photon pairs in the state $|\psi\rangle = \frac{1}{\sqrt{2}}(|H\rangle_a|V\rangle_b - |V\rangle_a|H\rangle_b)$. There is a probability that both sources will produce a photon pair from the same pulse. We post-select the cases where there is a detection by all detectors. This can happen in one of two ways:

- Horizontal photons in modes b and c. In this case, the final state is $|H\rangle_1|H\rangle_2|V\rangle_3$.
- Vertical photons in modes b and c. In this case, the final state is $|V\rangle_1|V\rangle_2|H\rangle_3$.

So the final state is:

$$|\psi\rangle = \frac{1}{\sqrt{2}}\left(|V\rangle_1|V\rangle_2|H\rangle_3 + |H\rangle_1|H\rangle_2|V\rangle_3\right). \tag{2.14}$$

Note that this setup is actually producing a four photon GHZ state, but it can be used just as well to produce a three photon entangled state. This method has the advantage that it works 50% of the time[2], which is four times better than using double pairs from a single emitter. It does however still rely on post-selection.

GHZ state by interfering an entangled source with a coherent state

Finally, we will briefly mention a third way of producing three photon GHZ states. This method, shown in Figure 2.7, was proposed by Rarity at al. in [52], and was implemented in [53]. It involves a scheme similar to the one described in Figure 2.6, except that one of the entangled sources is replaced with a coherent state. The argument as to why this produces a GHZ state is the same as when two independent SPDC sources are interfered.

[2]A four photon GHZ state is produced 50% of the time. To obtain 50% success probability in the three-photon case, active switching with feed-forward is required.

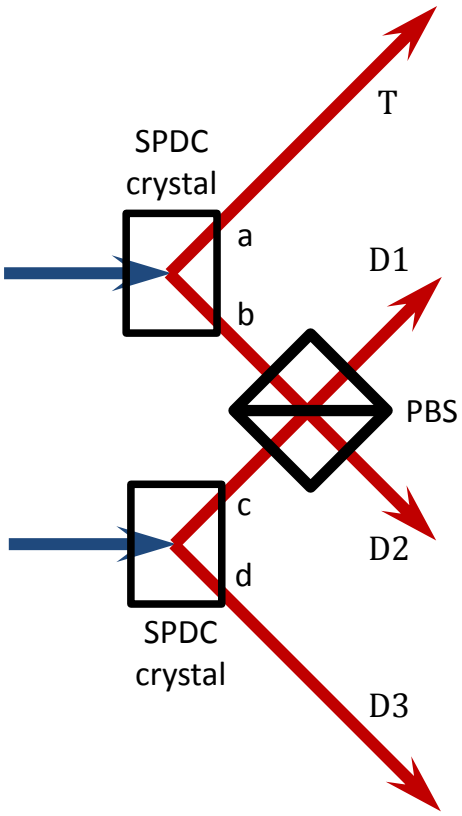

Figure 2.6: Setup for production of GHZ state by interfering two independent SPDC sources. Two nonlinear crystals are pumped by a pulsed laser to produce entangled pairs. The photons in modes b and c are interfered together on a PBS. If one of the outputs is used as a trigger and only four-fold coincidences are considered, then the result is a three photon GHZ state.

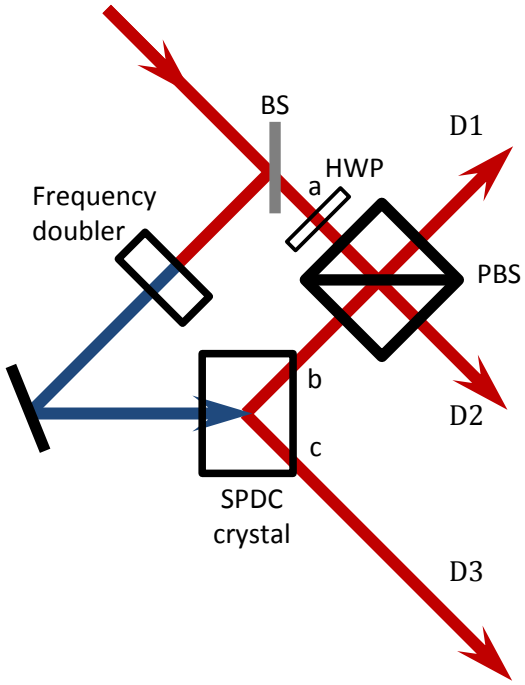

Figure 2.7: Setup for production of GHZ state by interfering an SPDC source with a coherent state. A pulsed laser beam passes through a beam splitter (BS). One part is frequency-doubled and then used to pump a source of entangled pairs. The other part's polarization is set to 45° with a HWP and is then interfered on a beam splitter with one of the photons from the pair. By post-selecting on three-folds, the result is a GHZ state.

If we ignore double pairs emitted by the entangled source, and if the coherent state in mode a is weak enough, then the dominant way to obtain a three-fold coincidence is for the photons in modes a and b to have the same polarization. The photon in mode c must have orthogonal polarizations. The state produced is thus of the form:

$$|\psi\rangle = \frac{1}{\sqrt{2}} \left(|V\rangle_1 |V\rangle_2 |H\rangle_3 + |H\rangle_1 |H\rangle_2 |V\rangle_3 \right) \tag{2.15}$$

The advantage of this method is that it allows for much higher count rates, because it does not require two separate down-conversions to happen at the same time. However, it still

requires post-selection. It also has a downside compared to the other schemes: it cannot lead to states with as high a fidelity. This is because because unlike the other schemes, there is no trigger detector, so there are more accidental coincidences[53].

2.2.2 W states

The first method used to produce W states using SPDC [54, 55] is shown in figure 2.8. A SPDC source is set up to produce $|\psi\rangle = \frac{1}{\sqrt{2}}(|H\rangle_a|V\rangle_b - |V\rangle_a|H\rangle_b)$ entangled states. We consider only the cases where all four detectors fire, and assume that a double pair was emitted. For this to happen, there needs to be exactly one horizontal photon and one vertical photon in mode a to get a detection at T, and one vertical photon reflected by the PBS. Consequently, there must be one horizontal and one vertical photon in mode b. The polarization dependant beam splitter (PDBS) has transmission $T_V = 2T_H$, so that 1/3 of the time, the horizontal photon is transmitted to D3. Photons reflected by the PDBS and the PBS are recombined probabilistically with a beam splitter, and then split up again to be detected by D1 and D2. This leads to the following state:

$$|\psi\rangle = \frac{1}{\sqrt{3}}(|V\rangle_1|V\rangle_2|H\rangle_3 + |V\rangle_1|H\rangle_2|V\rangle_3 + |H\rangle_1|V\rangle_2|V\rangle_3) \tag{2.16}$$

which is a W state.

Just like for GHZ states, there are several other methods that have been used to produce W states [56, 57], but we will not describe all of them in detail. The important point is that they all of them require post-selection. In Section 2.1, we mentioned that there was a fundamental change with the type II SPDC single emitter scheme, because it was the first method that created pairs of photons *directly, without post-selection* (as explained in Footnote 1). For three photon entanglement, an analogous step has not yet been achieved. In chapter 4, we describe an experiment where we have directly produced triplets, which we predict can be entangled without the use of post-selection.

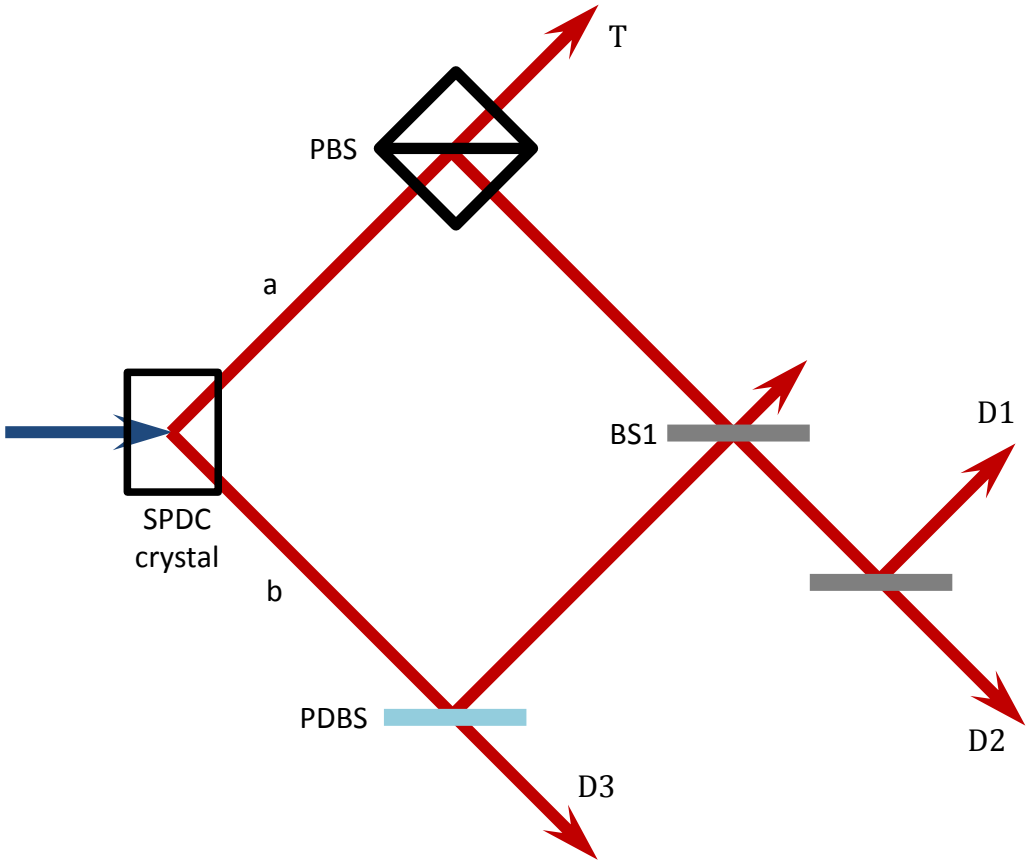

Figure 2.8: Setup for production of W state using double pairs from a single emitter. A SPDC source is pumped using a pulsed laser to produce entangled pairs. In the case where a double pair is emitted, the PBS takes out one horizontal photon, leaving one horizontal and two vertical photons. The polarization dependant beam splitter (PDBS) assures that the probability of the horizontal photon going to D1, D2 or D3 is equal in the cases where all four detectors fire.

Chapter 3

Experimental realization of a Sagnac source

3.1 Motivation

As we have seen in Section 1.4, quasi-phasematched materials allow for much better down-conversion efficiencies. However, the best way to make use of quasi-phasematched materials is through collinear down-conversion. Therefore, as we saw in Section 2.1, entangled photon source schemes based on cone geometries [8, 42] cannot fully benefit from quasi-phasematching.

The challenge when using collinear down-conversion is separating the down-converted photons that are created in the same spatial mode. One possibility, if the down-conversion is non-degenerate, is to use dichroic mirrors [44, 58] to separate them. However, this is obviously not possible when operating near degeneracy. Another option is simply to split up the photons probabilistically with a beam splitter [59], but this leads to the unwanted loss of half of the pairs. These losses can be avoided by using the interferometric schemes described in Section 2.1.4, but these configurations are limited by phase stability and therefore require active phase stabilization.

To avoid the need for active phase stabilization, it is possible to instead use a single down-converter, pumping it in two opposite directions inside a polarizing Sagnac interfer-

ometer. This idea was first realized in [60], albeit with type I SPDC, and so the down-conversion was not split into separate spatial modes. It was Kim et al. [61] who first showed an entangled source with a type II emitter inside a Sagnac interferometer. This setup was then improved in [62, 63]. Because this method uses collinear down-conversion, and does not require phase stabilization, these sources have been able to achieve high entanglement quality, while also allowing for a high source brightness. It also has the added advantage over other interferometric schemes that only one down-converter is required.

3.2 Theory

The Sagnac source is illustrated in Figure 3.1. A nonlinear crystal is placed in the middle of a polarizing Sagnac interferometer. The crystal is kept at a constant temperature appropriate for degenerate type II down-conversion of a horizontally polarized pump ($|H_\mathrm{p}\rangle \rightarrow |H_\mathrm{s}\rangle, |V_\mathrm{i}\rangle$, where the subscripts p, s and i represent the pump, signal, and idler photons respectively). The polarization of the pump is set using a half-wave plate and a quarter-wave plate (HWP1 and QWP1). The vertical component of the pump is reflected by the PBS, and is then rotated by the dual wavelength half-wave plate HWP3[1], which is set to 45°. This leads to pairs $|H_\mathrm{s}\rangle_\mathrm{a}, |V_\mathrm{i}\rangle_\mathrm{a}$ propagating clock-wise through the interferometer in mode a. These are split by the PBS, so that we have $|H_\mathrm{s}\rangle_\mathrm{c}, |V_\mathrm{i}\rangle_\mathrm{d}$. The horizontal component of the pump is transmitted by the PBS, and thus produces pairs $|H_\mathrm{s}\rangle_\mathrm{b}, |V_\mathrm{i}\rangle_\mathrm{b}$ propagating counter-clockwise through the interferometer in mode b. After HWP3, these become, $|V_\mathrm{s}\rangle_\mathrm{b}, |H_\mathrm{i}\rangle_\mathrm{b}$, and after the PBS, we have $|V_\mathrm{s}\rangle_\mathrm{c}, |H_\mathrm{i}\rangle_\mathrm{d}$. If the polarization state of the pump is a coherent superposition of $|H\rangle$ and $|V\rangle$, then the two photon state in modes c and d is: $\alpha|H_\mathrm{s}\rangle_\mathrm{c}|V_\mathrm{i}\rangle_\mathrm{d} + \beta e^{i\phi}|V_\mathrm{s}\rangle_\mathrm{c}|H_\mathrm{i}\rangle_\mathrm{d}$. α and β are set using HWP1, whereas the phase ϕ is controlled by tilting QWP1, which is at 0°. Note that because HWP3 also acts on the down-converted photons, both signal photons come out in mode c, and both idler photons exit through mode d. This allows the source to be operated in a non-degenerate regime. This also cancels out any problems from longitudinal walk-off caused by birefringence in the crystal, which is a common problem in sources using type II down-conversion [63]. We will elaborate on this point in section 3.4.4.

[1] HWP3 is a dual wavelength half-wave plate, meaning that it acts as a half-wave plate for two wavelengths: the pump's and the down-conversions's.

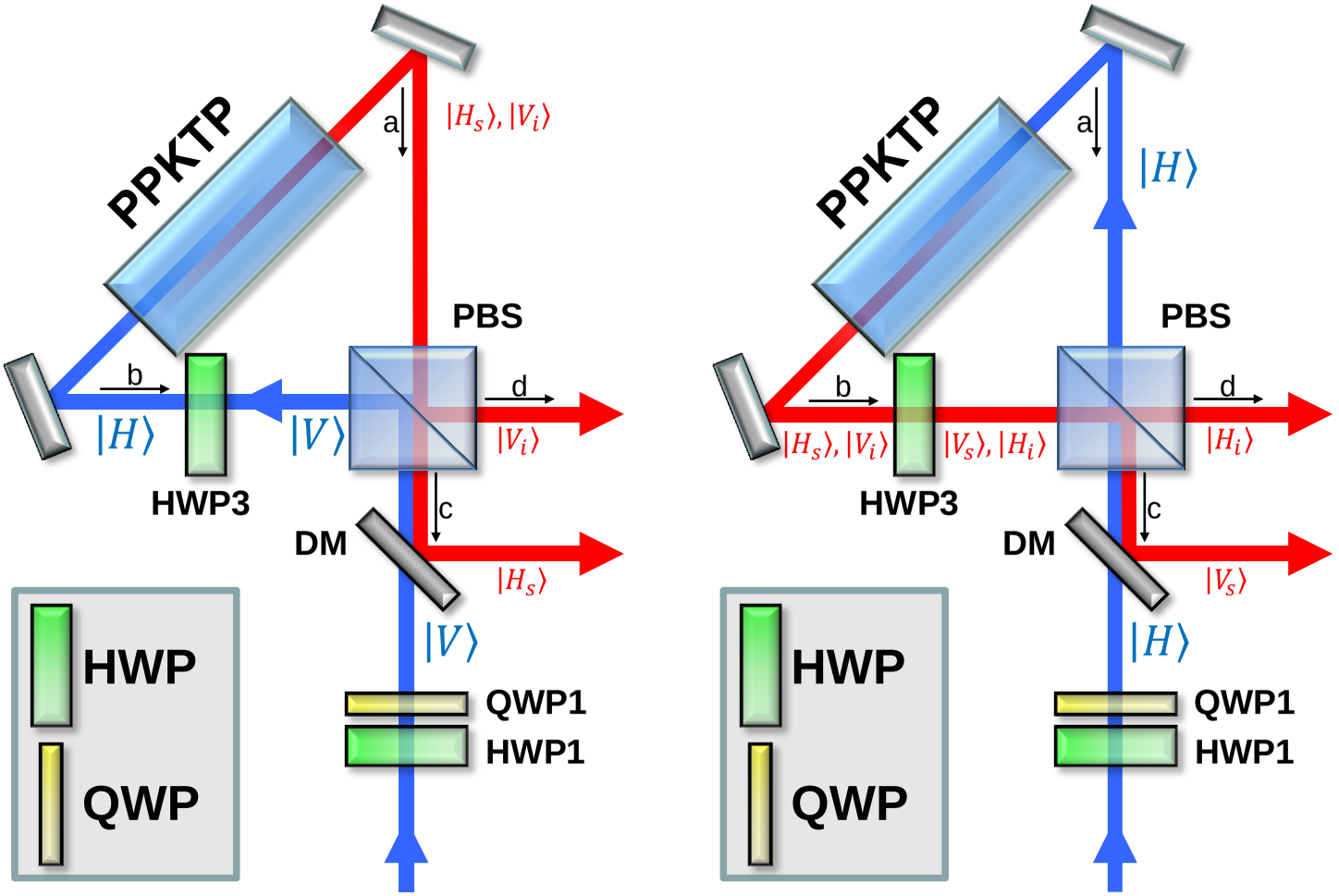

Figure 3.1: Illustration of the Sagnac Source of entangled photons. The pump is shown in blue, and the down-converted photons in red. The letters a, b, c and d indicate the spatial modes corresponding to all four ports of the PBS. The figure on the left shows the source when the pump is horizontally polarized, and the one on the right shows the source when the pump is vertically polarized. To produce an entangled state, we use a coherent superposition of these two cases.

3.3 Experimental methods

The setup of the Sagnac source is shown in Figure 3.2. The pump laser is a 404.5nm grating-stabilized laser diode (iWAVE-405-S, from Toptica Photonics). The produced beam is passed through a free-space optical isolator (IO-5-405-LP, from Thorlabs) in order to avoid retro-reflecting light into the laser. The pump beam is focused using a lens with a 200mm focal length. The nonlinear material is a 25mm crystal of periodically-poled potassium titanyl phosphate (PPKTP), with a grating period of 9.825 microns (from Raicol Crystals), which is kept inside an oven at a constant temperature appropriate for degenerate SPDC (between 50°C and 70°C, depending on the PPKTP sample). The down-converted photons are coupled into single mode fibers using achromatic lenses with a 30mm focal length. A guide detailing the construction and the alignment of the setup is provided in Appendix A.

The photons are detected using silicon avalanche photo-diodes, (PerkinElmer four-channel SPCM-AQ4C modules). These detectors have a detection efficiency of between 45% and 50% at 809nm [64]. To find coincidences, we use a homemade logic module, built by Zhenwen Wang of the University of Waterloo Science Technical Services, which outputs a signal when it receives TTL signals from each single photon detector within a time window of 6ns. Both the single photon detections and coincidences are recorded on a computer.

3.4 Results

3.4.1 Phasematching curves

We first show the effect of changing the PPKTP crystal's temperature on the spectrum of the down-converted photons. The results for a 10mm PPKTP crystal are shown in Figure 3.3.

These results illustrate one of the main advantages of quasi-phasematching for SPDC: easy tunability. Indeed, by changing the temperature of the PPKTP crystal in a range of

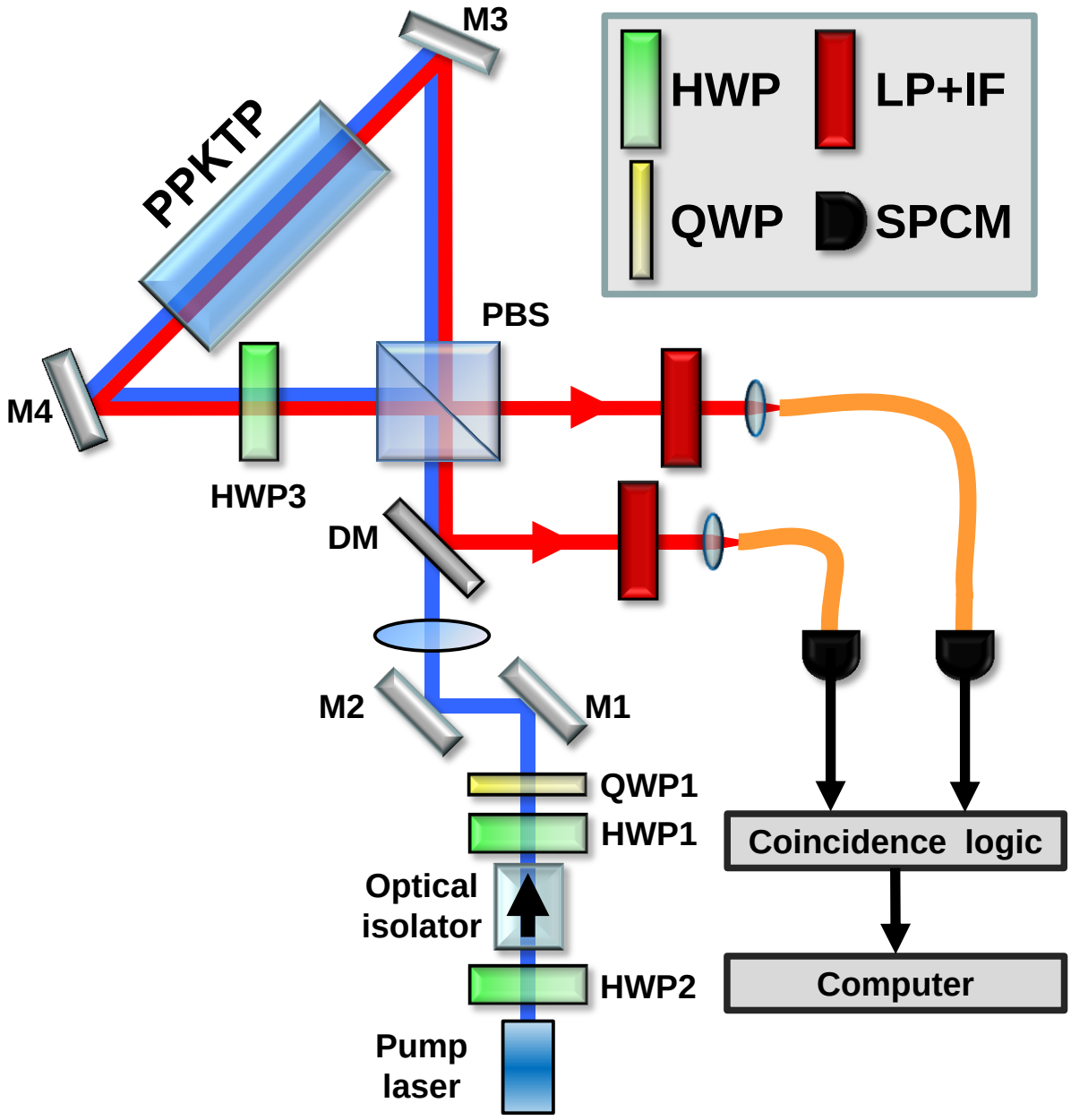

Figure 3.2: Experimental setup of the Sagnac source of entangled photons. After passing through the optical isolator, the pump beam's polarization is set by a half-wave plate (HWP1) and a quarter-wave plate (QWP1). It is then focused onto the PPKTP crystal. Single photons are separated from the pump using a dichroic mirror (DM). Any stray pump is removed using a low-pass filter (LP) and an interference filter (IF). The single photons are detected with single photon counting modules (SPCM). The output from the SPCM is then sent to a coincidence logic, who's output is analyzed on a computer.

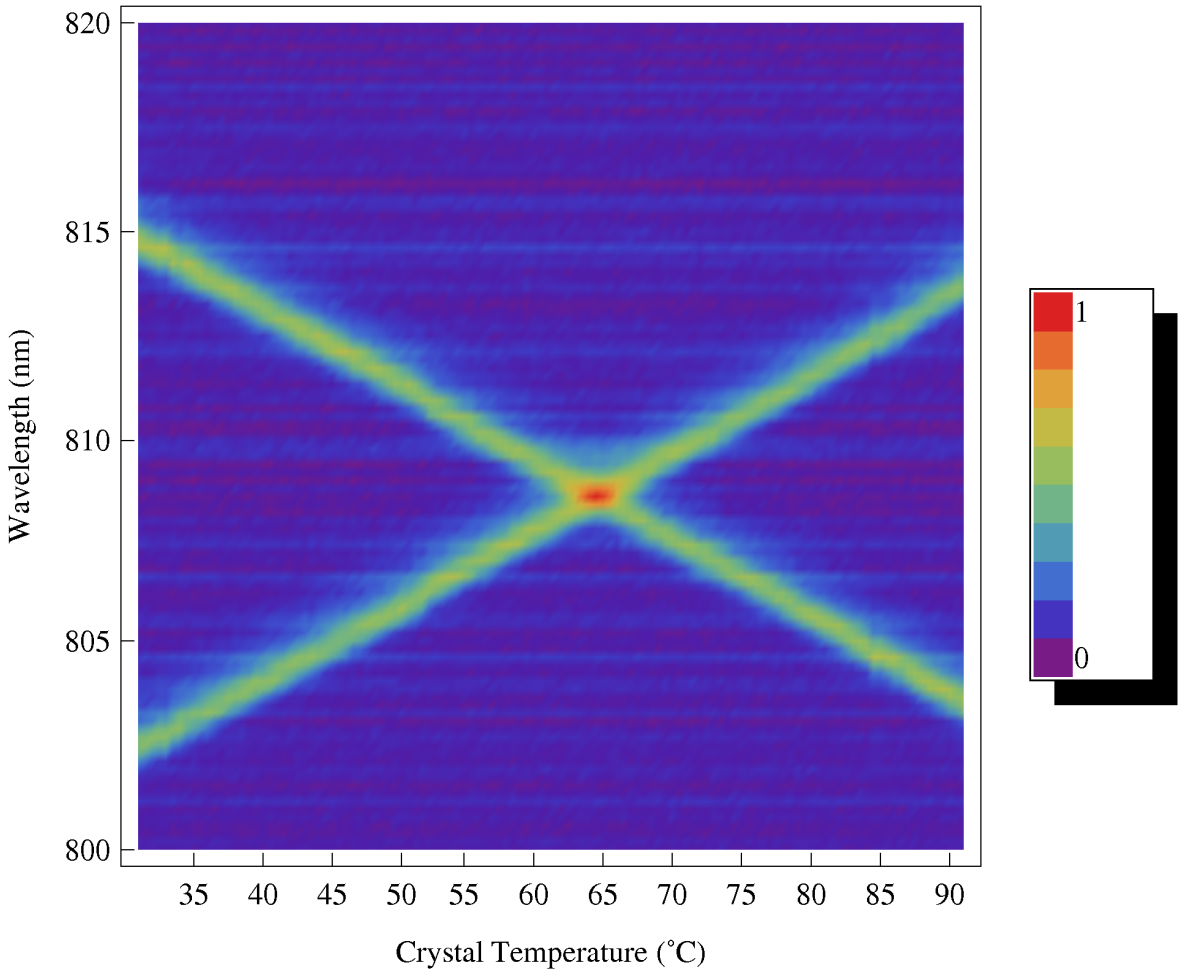

Figure 3.3: Phasematching curves for 10mm PPKTP crystal. This false color image shows the measured spectrum of the photons produced by SPDC for a range of temperatures. The measured intensity has been normalized. The line with the positive slope is the signal, whereas the one with the negative slope is the idler.

about 30°C, we can vary the wavelength of the down-converted photons by approximately 6nm. It is interesting to compare this with the theoretical predictions. To obtain the theoretical phasematching, we need to solve Equation 1.32, taking into account the proper temperature dependance of each term. This is detailed in Appendix B. The result is shown in Figure 3.4. The degeneracy points are very close to the one measured (66.8°C calculated, 64.5°C measured). However the slopes of the tuning curves differ a bit. We calculated an average slope of -0.218nm/°C for the idler, and measured -0.185nm/°C. This difference could be due to imperfections in the polling periods of the crystals, as we have noticed that the phase matching curves are not the same for every sample.

3.4.2 Source performance

With a 25mm PPKTP crystal pumped with 6mW (measured after the optical isolator), the source produced approximately 1,000,000 singles per second in each of its outputs, and 210,000 coincidences per second. The bandwidth of the down-converted photons, shown in Figure 3.5, was approximately 0.3nm. From these results, we can calculate the spectral brightness of the source to be 117000 pairs/s $\cdot$ mW $\cdot$ nm. This is a factor of 2.4 less than what is reported in [63]. This is partly due to power losses between where we measured the pump power (after the optical isolator) and the PPKTP crystal, mainly from the backside of the dichroic mirror and the PBS. However, the main contribution is that space constraints prevented us from achieving the optimal pump spot size in the crystal, something which was done in [63].

3.4.3 Characterization using quantum state tomography

To characterize the source, we used an external setup, capable of making any separable projective measurement on each of the photons. In this setup, the single photons are coupled back out into free-space, and then pass through a quarter-wave plate, a half-wave plate and a polarizing beam splitter. The wave plates are mounted in motorized rotation stages from Newport (PR50CC), which are controlled using a Newport XPS Universal High-Performance Motion Controller/Driver. All the measurements needed to perform quantum state tomography are automated with Labview, using a program written by

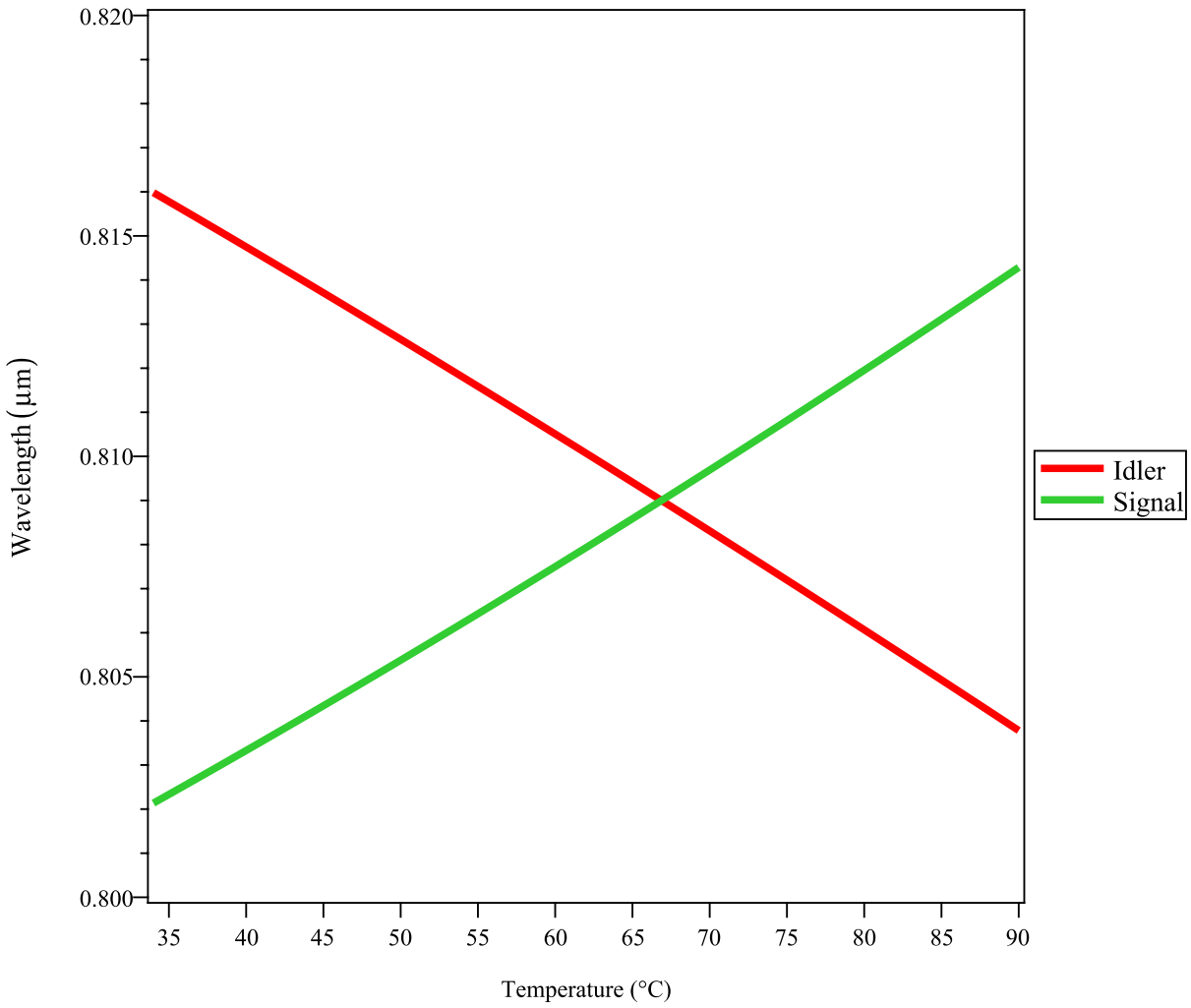

Figure 3.4: Theoretical phasematching curves for our PPKTP sample.

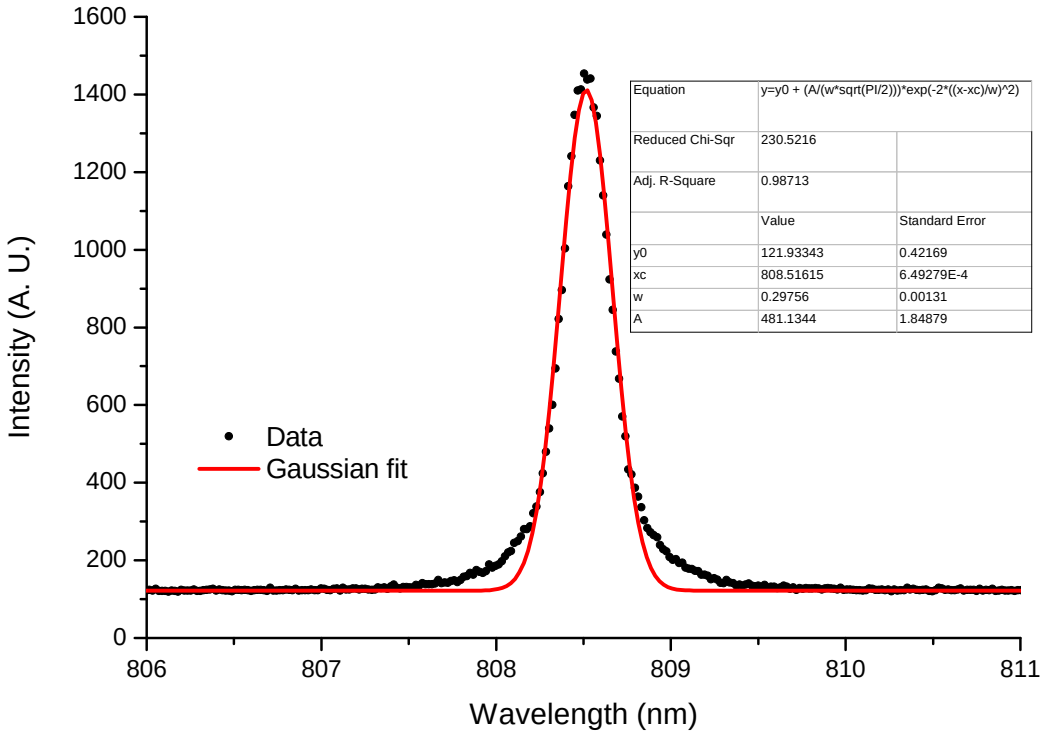

Figure 3.5: . Measured down-conversion spectrum in Sagnac source. From the Gaussian fit, we find that the bandwidth is approximately 0.3nm.

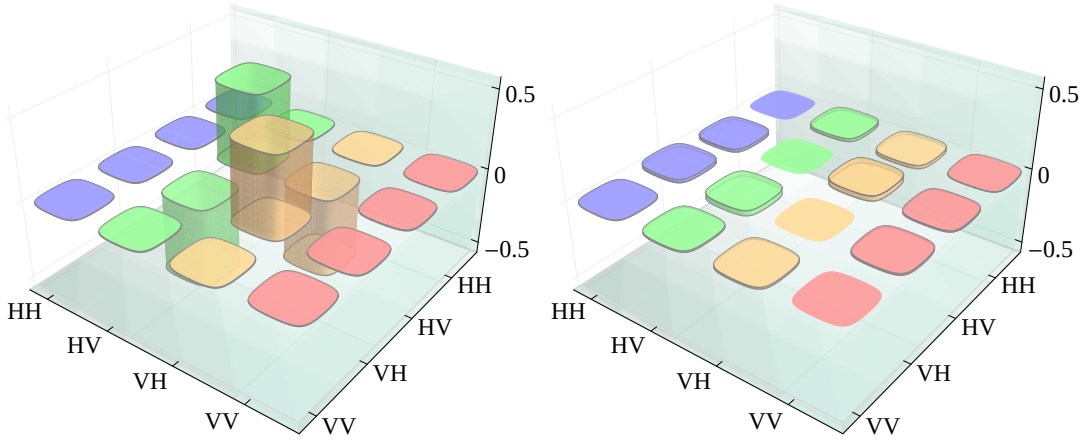

Figure 3.6: Reconstructed state measured with quantum state tomography. The left bar chart shows the real part of the reconstructed density matrix, whereas the right part shows the imaginary part. For ad ideal $|\psi^-\rangle$, every element of the density matrix should be 0, except for the four middle elements in the real part which would be either 0.5 or -0.5.

Rainer Kaltenbaek. The density matrix is reconstructed using the maximum likelihood method described in Section 1.2.2.

The reconstructed density matrix of a typical state is shown in Figure 3.6. In this example, the state was set to produce $|\psi^-\rangle$. The power of the pump was also set using HWP2 (see Figure 3.2), so that the coincidence rate was approximately 2000Hz. The tomography consisted of three cycles of 36 measurements, specifically all combinations of $|H\rangle$, $|V\rangle$, $|D\rangle = \frac{1}{\sqrt{2}}(|H\rangle + |V\rangle)$, $|A\rangle = \frac{1}{\sqrt{2}}(|H\rangle - |V\rangle)$, $|R\rangle = \frac{1}{\sqrt{2}}(|H\rangle - i|V\rangle)$ and $|L\rangle = \frac{1}{\sqrt{2}}(|H\rangle + i|V\rangle)$ measurements, each lasting 1 second.

In Table 3.1, we give several figures of merit of the reconstructed quantum state. The fidelity is a measure of how similar two states, τ and σ, are. It is given by: $F(\tau,\sigma) = \left[\mathrm{Tr}\left(\sqrt{\sqrt{\tau}\sigma\sqrt{\tau}}\right)\right]^2$ [65]. The purity of a state σ is given by : $\mathrm{Tr}[\sigma^2]$. The tangle is a measure of a two-qubit state's entanglement, which ranges from 0 for a separable state to 1 for a maximally entangled state (see [66] for more details). The error bars quoted are based on a Monte-Carlo simulation with 100 iterations. In each iteration, Poissonian noise is added to the counts, and the maximum likelihood routine is run. For this calculation, we used Mathematica code written by Robert Prevedel.

Property	Measured Value
Fidelity with $\|\psi^-\rangle$	0.9893 ± 0.0005
Purity	0.983 ± 0.001
Tangle	0.959 ± 0.002

Table 3.1: Figures of merit of reconstructed state

3.4.4 Effect of the crystal's position inside the interferometer

We have observed that the entanglement quality of the source is highly dependent on whether the crystal is properly placed inside the interferometer. To show this effect, we set the source to produce a $|\psi^-\rangle$ state so that the measurements in the diagonal basis should be anti-correlated. Then, with both of our analyzers set to $|D\rangle$, we measured the number of coincidences in 10 seconds. Ideally, it should be zero. We repeated the measurement as the crystal was translated along the direction of propagation of the beam. The result of this measurement is shown in Figure 3.7. We can see that when the crystal moves in either direction, the number of coincidences becomes higher. This translates to a lower entanglement visibility when the crystal is not in the optimal position.

We believe the effect can be explained in the following way. PPKTP is birefringent, and the signal and idler do not have the same polarization. Therefore, they do not have the same velocity inside the crystal, and so there is a longitudinal walk-off between them. In a well aligned Sagnac, we do not have to worry about this, because the longitudinal walk-off is the same whether the pairs are traveling clockwise or counter-clockwise through the interferometer.

However, if the crystal is not centered, this is no longer the case. Indeed, the overlap between the mode in which the pairs of photons are produced and the fiber-coupled mode is best in the middle of the interferometer. Because of this, the detected pairs have a higher probability of coming from the middle of the interferometer. If the crystal is not perfectly centered, the pairs produced in one direction will therefore travel a larger average distance in the crystal than the ones produced in the other direction. The longitudinal walk-off caused by birefringence will then not be same in both directions, which will provide some distinguishability between the two different types of pairs and adversely affect the entanglement.

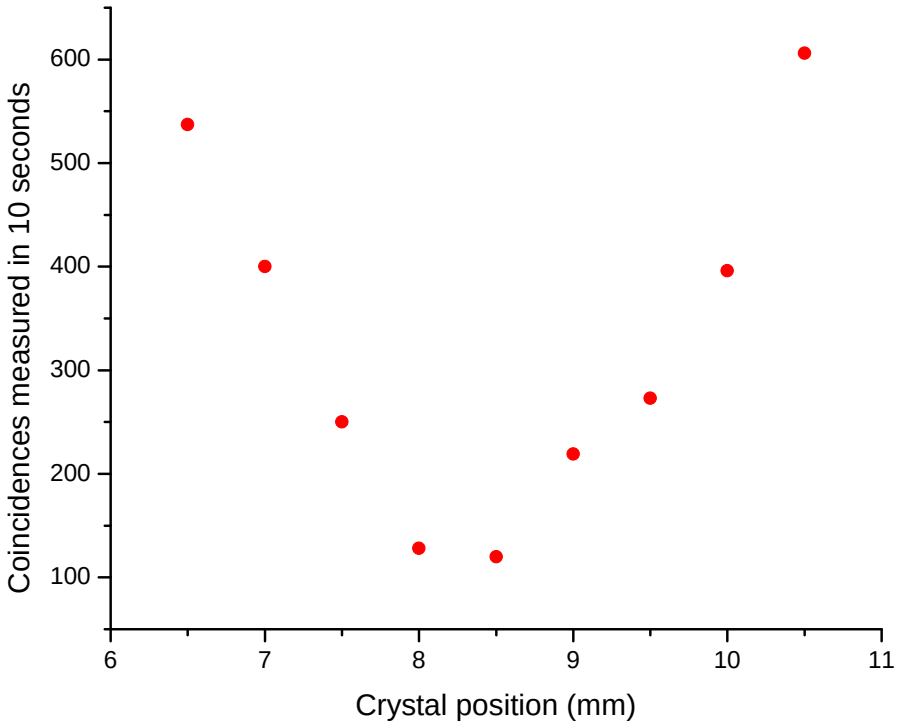

Figure 3.7: Effect of the crystal's position on entanglement. The points show the number of coincidences measured in 10 seconds with both analyzers set to $|D\rangle$, for different crystal positions. For an ideal $|\psi^-\rangle$, these should be zero. As the crystal moves away from its optimal position, the rate of measured coincidences increases, indicating a loss of entanglement. If one of the analyzers is set to do an $|A\rangle$ measurement, the coincidence rate was approximately 6000/10s, so the contrast in the diagonal basis goes from a minimum of $\sim 50:1$ to $\sim 10:1$.

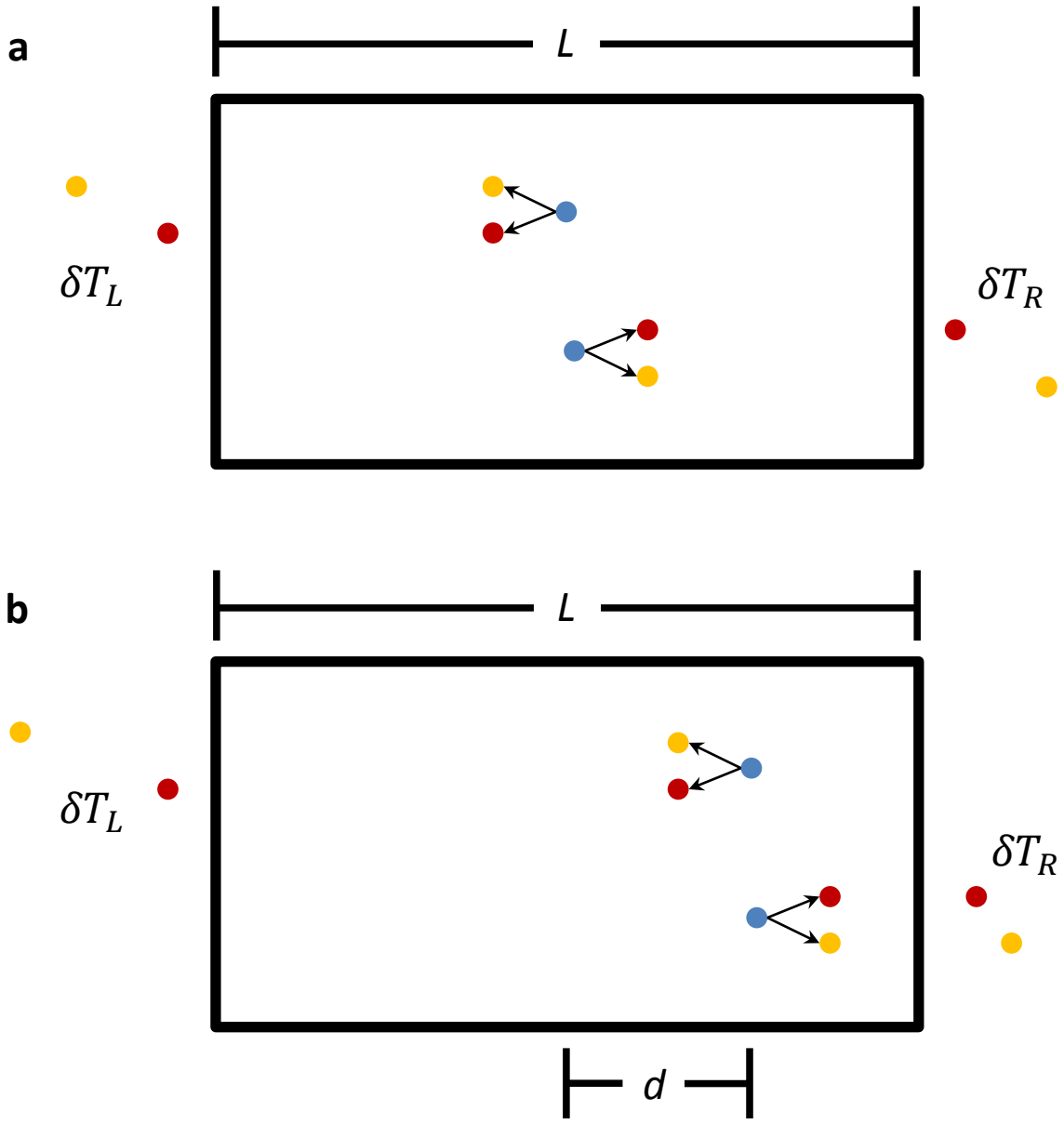

Figure 3.8: Time delays caused by birefringence. **a**, When the crystal is centered, the detected pairs are produced on average in middle of the crystal. The time delay δT between the signal (shown in orange) and the idler (shown in red) is the same for pairs produced in either direction. **b**, If the crystal is not centered, the detected pairs come on average from a distance d away from the center of crystal of length L. The delay is now larger for pairs traveling towards the left because these pair travels further on average inside the crystal.

We can do a rough calculation to check the plausibility of this explanation. Consider the situation shown in Figure 3.8b. When the pairs are traveling to the right, the signal will come out of the crystal ahead of the idler ahead by a time δT_R given by:

$$\delta T_R = \frac{(L/2 - d)}{c}(n_{gs} - n_{gi}) \tag{3.1}$$

where c is the speed of light, and n_{gs} and n_{gi} are the group velocity refractive indices for the signal and idler respectively. These can be calculated using the Sellmeier equations contained in Appendix B. We used $n_{gs} = 1.806$ and $n_{gi} = 1.912$. In the left direction, the time delay is:

$$\delta T_L = \frac{(L/2 + d)}{c}(n_{gs} - n_{gi}) \tag{3.2}$$

so the difference between the time delays in each direction, δT is given by:

$$\delta T = \delta T_L - \delta T_R = \frac{2d(n_{gs} - n_{gi})}{c} = l \cdot 0.71\text{ps/mm} \tag{3.3}$$

The pairs become distinguishable when δT is on the order of the coherence time of the single photons τ_c [8]. We can estimate their coherence time from their bandwith, measured to be 0.3nm.

$$\tau_c \approx \frac{\bar{\lambda}^2}{c\Delta\lambda} = 7.27\text{ps} \tag{3.4}$$

This means that a translation of only 1 cm would cause the relative time delay to be of the same order of magnitude as the coherence length. We should note that this model is quite simplistic. We have assumed that the photons are created only in a single point in the crystal, so we overestimate the dependance on position. Nonetheless, since the orders of magnitudes are correct, it is very probable that birefringence is indeed the cause of the loss of entanglement. More experiments are needed to confirm our hypothesis. The most direct way would be to add an additional birefringent material on one side of the interferometer, and then to see how the optimal position of the crystal is affected.

3.4.5 Effect of pump power on the state's entanglement quality

The tomography results in Section 3.4.3 were taken with the source operating at a relatively low power. The reason for this is that at higher powers, the measured fidelity drops significantly. A measurement of this effect is shown in Figure 3.9.

This is due to what we commonly call *accidental coincidences*. Indeed, as the number of counts measured becomes higher, the odds of two uncorrelated photons getting detected within the coincidence window of the logic increases also. More precisely, the rate of accidental coincidences, C_{acci} can be approximated by:

$$C_{\text{acci}} \approx S_1 S_2 W \tag{3.5}$$

where S_1 and S_2 are the number of detections per second at each detector, and W is the time window in which two detections will be deemed a coincidence by the logic. This can be rewritten as:

$$C_{\text{acci}} \approx R_{\text{pairs}}^2 \eta_1 \eta_2 W. \tag{3.6}$$

R_{pairs} is the number of photon pairs produced per second in the PPKTP crystal, and η_1 and η_2 are the respective coupling efficiencies of each channel. The number of "real" coincidences measured, C is given by:

$$C = R_{\text{pairs}} \eta_1 \eta_2 \tag{3.7}$$

Therefore, while the number of genuine coincidences detected increase linearly with R_{pairs}, the accidental coincidences increase by the square of R_{pairs}. This means that as the source is operated at higher powers, an increasing proportion of the coincidences measured are accidentals, thus explaining the loss of fidelity.

To verify that this explanation is valid, a simple calculation was used to predict the drop in fidelity that should arise because of these accidental coincidences. First, we set the

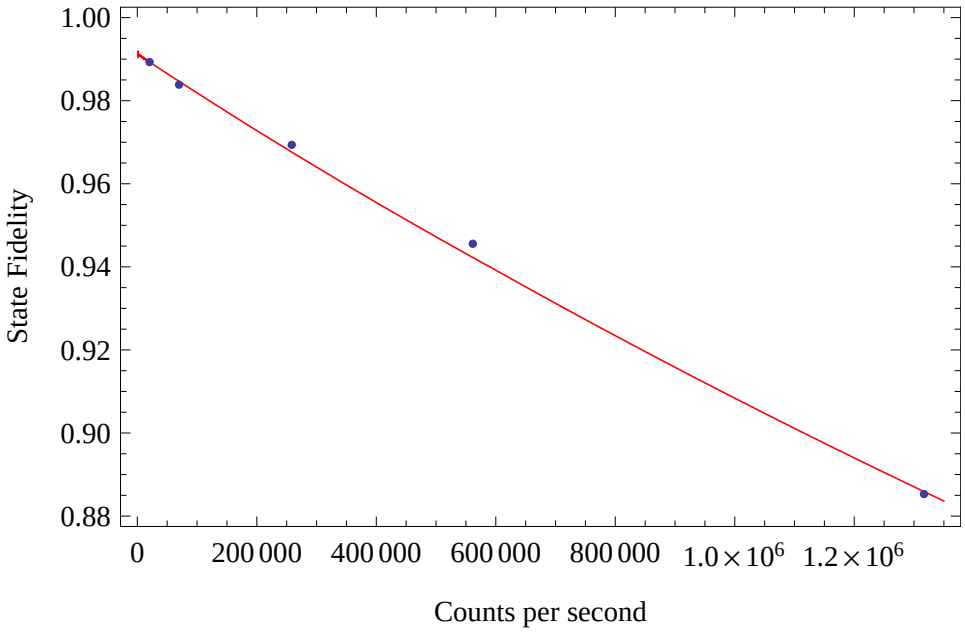

Figure 3.9: Effect of number the average number of detections per second on the theoretical and experimental fidelity with $|\psi^-\rangle$ of the produced quantum state. The predicted results are indicated by the red line, and the measured fidelities are the blue points.

source to produce a $|\psi^-\rangle$ state with very low count rates and performed an over-complete tomography. The number of expected accidental coincidences was calculated for all of these measurements. These calculated accidental counts were then subtracted from the measured data, in order to have an estimate of the number of real coincidences. Based on these, we extrapolated the number of both real and accidental coincidences that should be measured as the count rates are increased. Finally, we used a maximum likelihood reconstruction to find the quantum state most likely to correspond to these extrapolated measurements, and their fidelity with the ideal state $|\psi^-\rangle$. The results are shown in Figure 3.9. We can see that there is quite a good agreement between our empirical model and the measured results. This supports our claim that the loss in fidelity is mainly caused by accidental coincidences.

3.5 Applications

The source has been used for several experiments. As evidence of the contributions made possible by the work described in this thesis, we give here a list of experiments for which the source was used. However, since these experiments were not the main focus of this thesis, they will not be discussed in detail.

First, data from the source was used to investigate the challenges related to doing quantum key distribution with a very bright source of entangled photons. The idea is that, similarly to what was discussed in Section 3.4.5, as sources get brighter, there is a degradation in the effective secure bit rate. This can be attributed to double pair emission, i.e. two pairs produced within a short time, which is less than the coincidence window of the logic. The results were presented in:

- Chris Erven, Deny Hamel, Kevin Resch, Raymond Laflamme, and Gregor Weihs, Entanglement Based Quantum Key Distribution Using a Bright Sagnac Entangled Photon Source, In Quantum Communication and Quantum Networking (A. Sergienko, S. Pascazio and P. Villoresi, eds.), pp. 108-116, Springer, Berlin, 2010.

The source was also employed for an experiment on cluster state quantum computing. The goal was to study the benefit of using generalized quantum measurements (POVMs) instead of only projective measurements to enhance the computational power of a given the cluster state. This work was published in:

- Devon N. Biggerstaff, Rainer Kaltenbaek, Deny R. Hamel, Gregor Weihs, Terry Rudolph and Kevin J. Resch, Cluster-state quantum computing enhanced by high-fidelity generalized measurements, *Phys. Rev. Lett.* 103:240504, 2009.

Another experiment which used the Sagnac source, was done on the subject of remote state preparation[2]. The goal was to show that with shared entanglement and feed-forward, remote state preparation between two parties can be more successful than the classical threshold. The experimental results, as well as the theory to calculate these classical thresholds, was published in:

[2]The author of this thesis was note directly involved in this experiment

- Nathan Killoran, Devon N. Biggerstaff, Rainer Kaltenbaek, Kevin J. Resch, and Norbert Lütkenhaus, Derivation and experimental test of fidelity benchmarks for remote preparation of arbitrary qubit states, *Phys. Rev. A* 81:012334, 2010.

The next experiment investigated the state discrimination of entangled states using local polarization measurements and feed-forward. Our scheme achieved optimal state discrimination both with orthogonal and non-orthogonal states, and showed a distinct advantage with the use of feed-forward. The results of this experiment have been submitted for publication, and are currently available on the arXiv:

- Yang Lu, Nick Coish, Rainer Kaltenbaek, Deny R. Hamel, Sarah Croke and Kevin J. Resch, Minimum-error discrimination of entangled quantum states, arXiv:quant-ph/1008.0843, 2010.

Finally, the most recent experiment that used the source investigated the benefit of using entanglement when sending classical information over a noisy classical channel[3]. A manuscript describing the results from this experiment is currently in preparation.

[3]The author of this thesis was note directly involved in this experiment

Chapter 4

Direct generation of photon triplets using cascaded photon-pair sources

4.1 Notes and acknowledgements

In this chapter we describe the experimental production of photon triplets using cascaded spontaneous down-conversion. The motivation for this comes from what was explained in Section 2.2. Unlike for two photon entanglement, there is currently no way of producing three entangled photons without post-selection. This experiment is a step in that direction, by showing the first *direct* generation of photon triplets.

Notice: The content of this chapter has been published in :

Hannes Hübel, Deny R. Hamel, Alessandro Fedrizzi, Sven Ramelow, Kevin J. Resch and Thomas Jennewein, Direct generation of photon triplets using cascaded photon-pair sources. *Nature*, 466:601-603, 2010.

Author contributions

Hannes Hübel and **Deny R. Hamel** performed the experiment and analyzed the data

Alessandro Fedrizzi and **Sven Ramelow** participated in the design of the experiment

Kevin J. Resch and **Thomas Jennewein** contributed to the design and realization of the experiment

All authors co-wrote the paper.

4.2 Introduction

Non-classical states of light, such as entangled photon pairs and number states, are essential for fundamental tests of quantum mechanics and optical quantum technologies. The most widespread technique for creating these quantum resources is the spontaneous parametric down-conversion (SPDC) of laser light into photon pairs[67]. Conservation of energy and momentum in this process, known as phase-matching, gives rise to strong correlations which are used to produce two-photon entanglement in various degrees of freedom[5, 6, 8, 68, 69, 70, 71, 72]. It has been a longstanding goal of the quantum optics community to realise a source that can produce analogous correlations in photon *triplets*, but of the many approaches considered, none have been technically feasible[52, 73, 74, 75, 76, 77, 78, 79]. In this paper we report the observation of photon triplets generated by cascaded down-conversion. Here each triplet originates from a *single* pump photon, and therefore quantum correlations will extend over all three photons[80] in a way not achievable with independently created photon pairs[81]. We expect our photon-triplet source to open up new avenues of quantum optics and become an important tool in quantum technologies. Our source will allow experimental interrogation of novel quantum correlations[82], the post-selection free generation of tripartite entanglement[74, 83] without post-selection and the generation of heralded entangled-photon pairs suitable for linear optical quantum computing[84]. Two of the triplet photons have a wavelength matched for optimal transmission in optical fibres, ideally suited for three-party quantum communication[85]. Furthermore, our results open interesting regimes of non-linear optics, as we observe spontaneous down-conversion pumped by single photons, an interaction also highly relevant to optical quantum computing.

4.3 Theory

Given the potential for fundamental and applied quantum sciences, several physical systems have been proposed for the direct generation of photon triplets. These include four-level atomic cascades and higher-order optical nonlinearities[52], tri-excitons in quantum dots[73], combinations of second-order nonlinearities[75], and high-energy electron-positron collisions[76]. Extremely low interaction strengths and collection efficiencies have rendered these proposals unfeasible. Recent experiments have observed and studied third-order[77, 78] and cascaded second-order nonlinear[79] parametric processes seeded by strong lasers. However, such seeding only increases stimulated emission which masks the production of three-partite quantum correlations and cannot lead to three-photon entanglement.

Production of photon triplets by cascaded spontaneous parametric down-conversion (C-SPDC) was first proposed 20 years ago[74], yet never experimentally realised. The basic idea is shown in Fig. 4.1a. A primary down-conversion source is pumped by a laser to create a photon pair. One of the photons from this pair drives a secondary down-conversion process, generating a second pair and hence a photon triplet. Since the photon-triplet originates from a single pump photon, the created photons have strong temporal correlations[86] and their energies and momenta sum to those of the original photon.

The C-SPDC process can be described using a simplified quantum optical model. The interaction Hamiltonian for the primary source can be written as, $H_1 = \lambda_1 \alpha (a_0^\dagger a_1^\dagger + h.c.)$, with the pump laser treated as a classical field with amplitude α, and the photon creation operators of the two output modes $a_0^\dagger$ and $a_1^\dagger$. The coupling strength between the interacting fields is expressed by the parameter λ_1, which includes the nonlinear response of the material and governs the expected conversion rate of pump photons. For the second down-conversion, the pump field is now a single photon and must be treated quantum mechanically in the interaction Hamiltonian, $H_2 = \lambda_2 (a_0 a_2^\dagger a_3^\dagger + h.c.)$, with output modes 2 and 3. The evolution operator of the system is $U = U_2 U_1 = \exp(-iH_2)\exp(-iH_1)$, and can be approximated by expanding each term to first order. Applying U to the initial vacuum state and ignoring the vacuum contribution for the final state results in

$$\begin{aligned} |\Phi\rangle &= U|0_0, 0_1, 0_2, 0_3\rangle \\ &\approx -i\lambda_1\alpha|1_0, 1_1, 0_2, 0_3\rangle - \lambda_1\lambda_2\alpha|0_0, 1_1, 1_2, 1_3\rangle, \end{aligned} \tag{4.1}$$

where the subscripts label the spatial modes. The first term describes the pair creation process in the first crystal, while the second represents the desired three-photon state, $|0,1,1,1\rangle$, where the amplitude scales as the product of the two coupling strengths λ_1 and λ_2 of both down-converters. Note that Eq. 4.1 predicts that the rate of triplet production from C-SPDC should be linear in the intensity of the pump laser.

The conversion efficiencies in SPDC are typically very low. In optical nonlinear materials such as β-Barium Borate, for example, they reach about 10^{-11} per pump photon[87]. Major advances in nonlinear optics, such as quasi-phasematching of optical materials, have recently made it possible to access the inherent higher nonlinearities of materials such as periodically-poled Lithium Niobate (PPLN) and periodically-poled Potassium Titanyl Phosphate (PPKTP). The down-conversion efficiencies demonstrated in these materials can reach up to 10^{-9} in bulk[63]. The introduction of optical waveguides in photon-pair sources[88] has further increased conversion efficiencies to 10^{-6}, making the observation of C-SPDC possible.

4.4 Experimental methods

Figure 4.1b depicts the experimental setup (see Methods for more details). The primary source generated photon pairs in a PPKTP crystal, quasi-phasematched for collinear SPDC of 405 nm $\rightarrow$ 775 nm + 848 nm. The 775 nm photons were used to pump the secondary source, consisting of a PPLN waveguide, quasi-phasematched for 775 nm $\rightarrow$ 1510 nm + 1590 nm. The photon triplets were measured using a chained series of three photon counters (D1, D2 and D3) based on avalanche photo-diodes (APD). The detection of a 848 nm photon at D1, which occurred at a rate of about 1 MHz, opened a 20 ns gate at D2, which in turn gated D3 for 1.5 ns. The actual gate rate of D2 was reduced to 870 kHz, due to saturation. Since D3 was only armed if both D1 and D2 had fired, an event at D3 constituted the detection of a photon triplet. The temporal signature of these triple coincidences was recorded as histograms with a fast time acquisition card, where the detection signal of D1 served as the start trigger, and the detection signal on D3 as the stop. Data were recorded for a total of 20 hours, and analysed as a histogram of the time-interval between D3 and D1 detections, $\Delta\tau_{D3-D1}$.

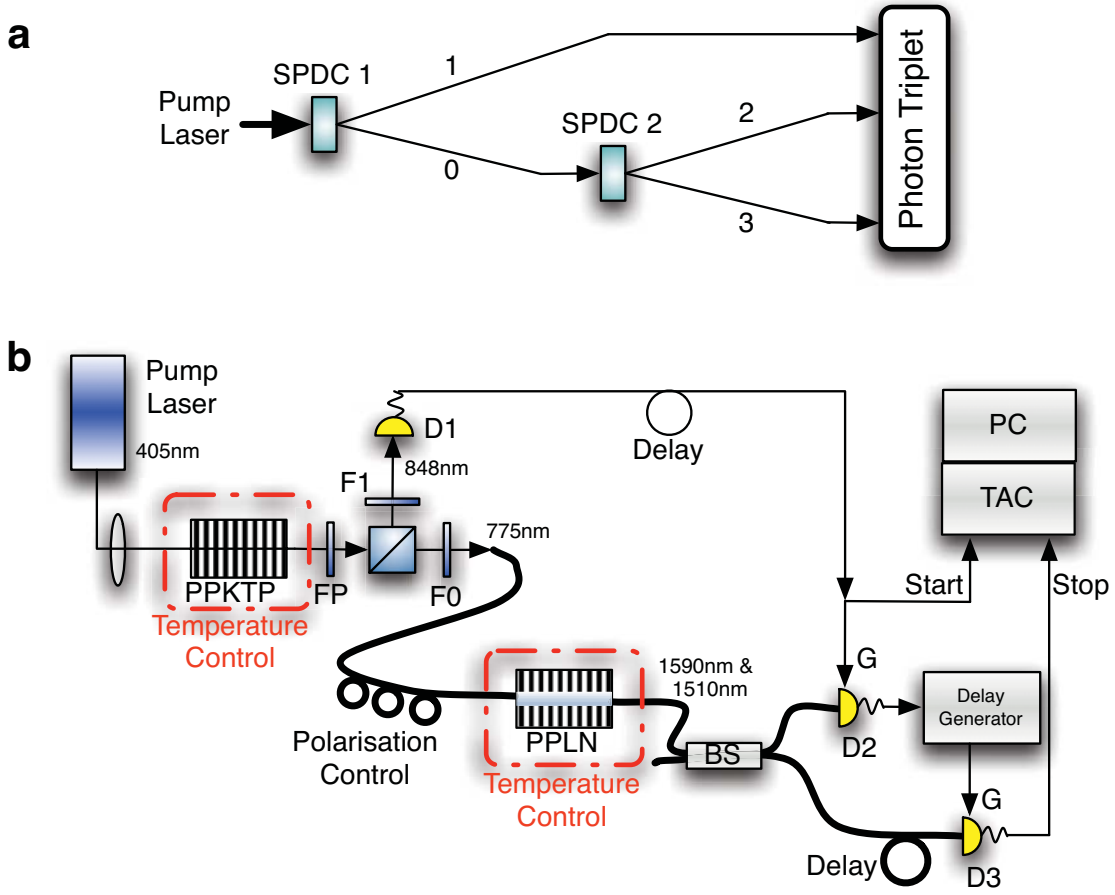

Figure 4.1: Schematic of photon triplet generation and experimental setup. **a**, A down-conversion source (SPDC1) produces a pair of photons in spatial modes 0 and 1, where the photon in mode 0 creates another photon pair in the second source (SPDC 2) in modes 2 and 3, generating a photon triplet. **b**, The primary source, pumped by a 405 nm laser, produces photon pairs at 775 nm and 848 nm. The 848 nm photon is directly detected by a silicon avalanche photo-diode (D1), while the 775 nm photon serves as input to the secondary source, creating a photon pair at 1510 nm and 1590 nm, which is detected by two InGaAs avalanche photo-diodes (D2 and D3). A detection event at D3 represents a measured photon triplet.

4.5 Results and analysis

A typical data set, shown as a histogram in Fig. 4.2a, displays a peak 8 standard deviations above the background noise. This is a clear signature of C-SPDC photon triplets. The 1.2 ns temporal width of the observed photon-triplet peak is dominated by detector jitter. Integration over the three central time bins yields a raw triplet rate of 124 ± 11 events in 20 hours. The observed background in the histogram is caused predominantly by triple events between a genuine detection in D1 and dark counts in D2 and D3 (see Methods) and was estimated from the displayed data to be 10.2 ± 0.9 per bin in 20 hours. The detected rate of triplets, exclusively produced by the C-SPDC process, was 4.7 ± 0.6 counts per hour. We modelled the process under the assumption that the down-conversion efficiency per photon in the secondary source was independent of the pump intensity (see Supplementary Information). Using the conversion efficiencies obtained from independent characterisations of both sources at mW pump power, and optical parameters from other relevant components of our setup, our model predicts a triplet rate of 5.6 ± 1.1 counts per hour, which is in very good agreement with the measured value.

It is expected that C-SPDC photon triplets should exhibit strict time correlations[86]. We investigated this property by introducing three different delays between D2 and D3 (-0.5, 0 and 0.5 ns) and measuring the histograms. The data in Fig. 4.2b shows a significant reduction of the peak in the histograms with additional delays, verifying the strong temporal correlations of the created triplets.

It is conceivable that other physical processes, such as the APD breakdown flash from D1[89], electronic cross-talk, or double-pair emission from the primary source, might give rise to correlated triple detection events with similar features to the ones we have observed. We can rule out these alternatives by testing the expected dependence of the C-SPDC signal on temperature and input wavelength of the secondary down-conversion. As shown in Fig. 4.3a, for a given input wavelength into the PPLN crystal, phase-matching imposes a minimum temperature below which down-conversion cannot occur. The triple coincidence peak, in Fig. 4.3b, indeed disappears when the PPLN temperature is lowered from 60°C (setting A) to 50°C (setting B), while keeping the input wavelength fixed at 776.0 nm. The triple photon signal is then recovered at this temperature, by lowering the input wavelength to 775.4 nm (setting C). These measurements, together with the strong agreement between

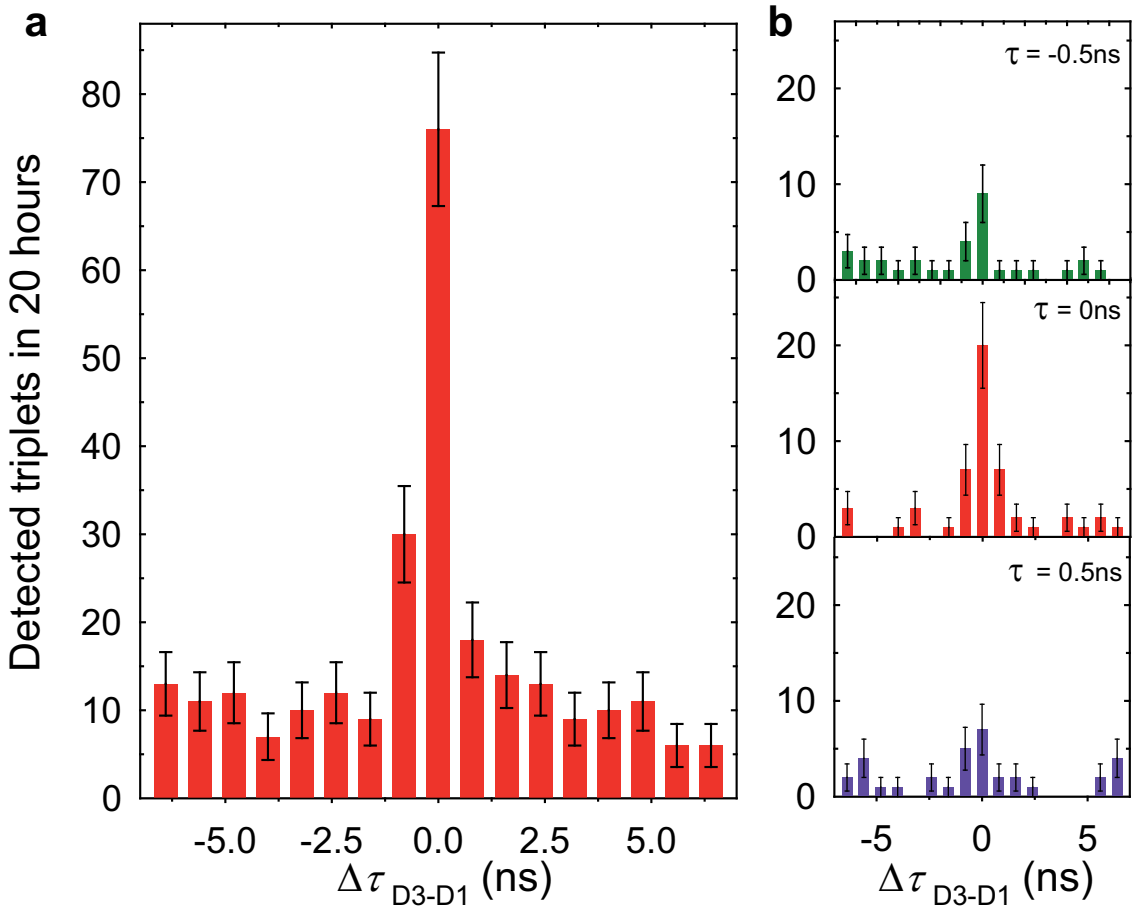

Figure 4.2: Triple-coincidence histograms. **a**, Measured triple coincidences obtained in 20 hours. Each bin corresponds to a 0.8 ns time interval between events at D3 and D1 ($\Delta\tau_{D3-D1}$). The sharp peak indicates a strong temporal correlation between all three detection events, as expected of the C-SPDC process. **b**, Triple-coincidence histograms with varying delays of $\tau = 0$ and ± 0.5 ns between D2 and D3, resulting in a decrease of the coincidence peak. Note that the absolute rate reduction for $\tau = 0$ results from a different setting on the InGaAs detectors for this measurement series. Error bars represent one standard deviation.

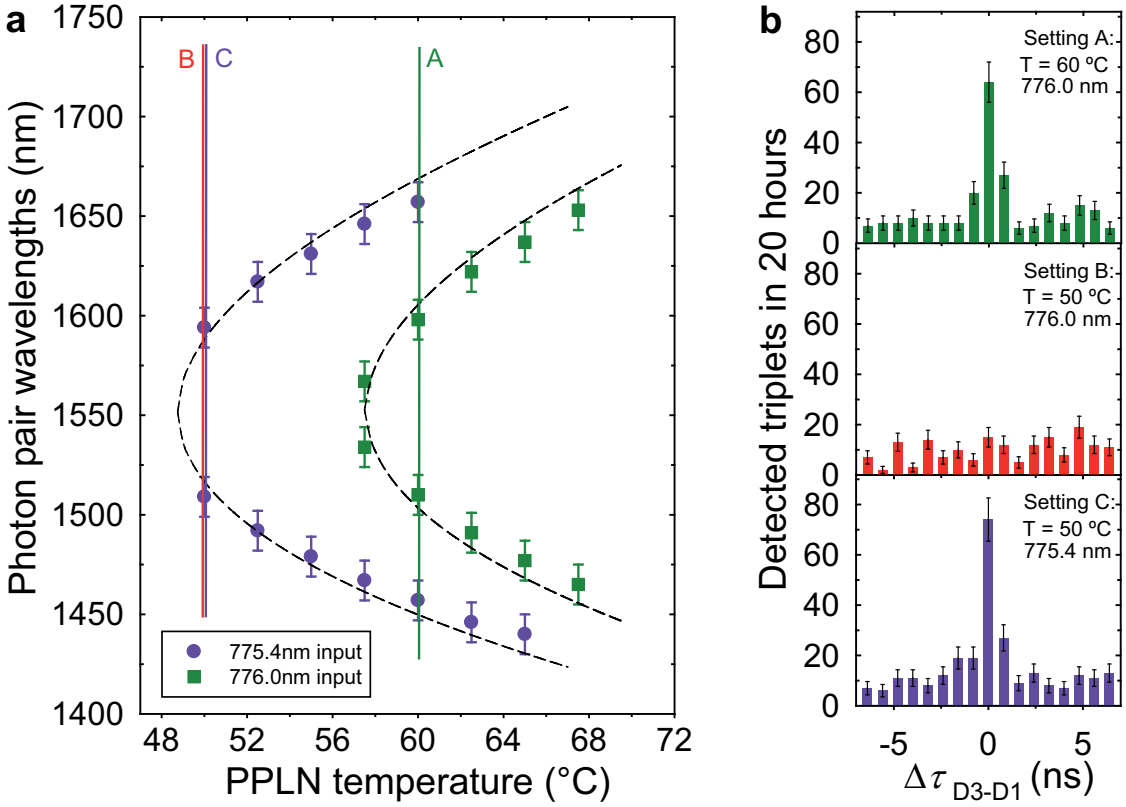

Figure 4.3: Phase-matching and triple-coincidence dependence on crystal temperatures. **a**, Central wavelengths of the pair of photons produced by the secondary source as a function of the PPLN temperature for input wavelengths of 775.4 nm (circles) and 776.0 nm (squares). The dashed line shows the theoretic phase-matching curve with the poling period as the only fit parameter. Triple coincidences were measured for different settings of the PPLN temperature and the input pump photon wavelength. The PPLN temperature was 60 C for setting A and 50 C for settings B and C; the input photon wavelength was 776.0 nm for settings A and B and 775.4 nm for setting C. **b**, Measured triple coincidence histograms over 20 hours for each measurement setting. For A and C, the PPLN temperatures lie on the respective phase-matching curves and a triple coincidence peak is observed. For B, the temperature is outside the 776.0 nm phase-matching curve and no peak is present. Wavelength changes in the input photons, needed for the measurements shown in Fig. 4.3b, were achieved by altering the temperature of the PPKTP crystal (43.6°C for setting A and B, and 40.8°C for C). Error bars represent one standard deviation.

the observed and predicted triplet rate, provide conclusive proof that we have indeed observed spontaneously produced photon triplets.

4.6 Conclusion and outlook

In the near future we expect to increase the photon-triplet rate by at least one order of magnitude using an improved time acquisition system, a dichroic beamsplitter for separating the photons created in the secondary source and matching the down-conversion bandwidth of the initial pair to the PPLN crystal. The direct generation of the triplet guarantees strong energy-time correlations, allowing the creation of entangled, or hyper-entangled[90] triplets and realisations of tri-partite states like GHZ[50] and W[54] without elaborate and probabilistic post-selection schemes. For example, time-bin entangled[69] GHZ states could be produced by pumping our triplet source with a pulsed pump laser in a coherent superposition of two time slots. The entanglement could then be detected using three standard unbalanced interferometers. For a further example, W-states could be made by using an entangling source as the primary down-converter producing a Bell-state $\frac{1}{\sqrt{2}}(|V_0V_1\rangle + |H_0H_1\rangle)$, where $|V\rangle$ and $|H\rangle$ denote the photon polarization states in their respective modes. The secondary source would consist of two down-converters where $|V_0\rangle$ is converted to $|H_2H_3\rangle$, and $|H_0\rangle$ is converted to $\frac{1}{\sqrt{2}}(|H_2V_3\rangle + |V_2H_3\rangle)$, into the same pair of modes. The relative amplitudes could then be balanced by tuning the conversion efficiencies. Polarization entangled GHZ states could be made by modifying the W-state scheme such that the secondary source converts $|V_0\rangle$ to $|V_2V_3\rangle$ and $|H_0\rangle$ to $|H_2H_3\rangle$. An interesting application of such a GHZ source could be to herald the presence of an entangled photon pair in mode 1 and 2 by detecting the secondary down-converted photon in mode 3. This has proven very difficult to achieve otherwise. Our results also confirm that the SPDC conversion efficiency is independent of pump power down to the single photon level (see Supplementary Information), allowing new tests of nonlinear optics in the quantum regime.

4.7 Methods summary

4.7.1 Experimental setup

The primary source, shown in Fig. 4.1b, consisted of a 25 mm long, temperature-stabilised PPKTP crystal and was pumped with 2.4 mW from a 405 nm continuous-wave diode laser. The type II SPDC in the PPKTP generated orthogonally-polarised photons at 775 nm and 848 nm, which were separated by a polarising beamsplitter and coupled into single mode fibers. A longpass filter (FP) was used to block the strong 405 nm pump, passband filters (12 nm bandwidth) with central wavelengths of 780 nm (F0) and 840 nm (F1) respectively, were placed before the fiber couplers to further reduce background. The 775 nm photon, after passing an in-fiber polarisation controller, served as input to the secondary source, a 30 mm temperature-stabilised PPLN waveguide crystal with fiber pigtails attached to both ends for type I SPDC. The photon pair at 1510 nm and 1590 nm was separated using a 50:50 fiber beamsplitter (BS). The secondary source was operated without filters, as the input power during a C-SPDC measurements was low enough ($\sim$ 1 million input photons per second) not to cause additional detection events in the InGaAs detectors. The gate (G) and photon arrivals on these detectors were synchronised by an internal delay generator on D2, and an external delay generator between D2 and D3. Detection efficiencies on the InGaAs detectors D2 and D3 were set to 20% and 10%, respectively. Trigger events from D1 and detection events from D3 were recorded via a time acquisition card (TAC) with a timing resolution of 103 ps and analysed on a computer (PC).

4.7.2 Dark count rate

The total background during the 20 hour runs, seen in Fig. 4.2a, was measured to be 268 $\pm$ 16 events over the whole 20 ns gate. This number is in very good agreement with the expected noise count of 254 $\pm$ 5 triple events as calculated from the individual dark count probabilities per gate of D2 and D3 (1.8×10^{-3} and 4.5×10^{-6}), trigger rate and efficiency of the time acquisition card.

4.8 Supplementary information

4.8.1 Calculation of the expected triplet detection rate

The predicted triplet rate, R_{triple}, quoted in our manuscript was calculated in the following way. Considering the efficiencies of all the components of the C-SPDC setup and the down-conversion probability, the triple coincidence probability (P_{triple}) per trigger at D1, is given by

$$P_{triple} = \eta_{775}\,\eta_{in}\,P_{SPDC}\,\eta_{out}^2\,2\,\eta_{BS}^2\,\eta_{D2}\,\eta_{D3} \tag{4.2}$$

where η_{775} is the fiber coupling probability of the primary SPDC, η_{in} and η_{out} are the coupling efficiencies into and out of the waveguide respectively, P_{SPDC} is the intrinsic down-conversion probability of the PPLN waveguide, η_{BS} is the transmission of the fiber beamsplitter for either arms, and η_{D2} and η_{D3} are the detection efficiencies of the InGaAs-APDs D2 and D3, respectively.

The probability, η_{775}, to find a 775 nm photon in the output fiber of the primary source upon detection of its partner photon at 848 nm was estimated from a coincidence measurement between the 775 and 848 nm photons, where a coincidence to singles ratio of 0.24 was measured. Assuming a detection efficiency of $\eta_{D1} = 0.45 \pm 0.05$ for the Si-APD (D1), the fiber coupling probability, η_{775}, is 0.53 ± 0.06.

The probability, P_{coinc}, of a detected coincidence event between the pair photons of the secondary source, given a single 775 nm photon in the input fiber of the waveguide, can be written as:

$$P_{coinc} = \eta_{in}\,P_{SPDC}\,\eta_{out}^2\,\eta_{LP}^2\,2\,\eta_{BS}^2\,\eta_{D2}\,\eta_{D3}\,\eta_{duty} \tag{4.3}$$

where η_{LP} is the transmission of a longpass filter needed to block the strong pump light and η_{duty} is the duty cycle of detector D2, which was operated in a quasi free running mode with 100 ns gate width and 100 kHz gate repetition rate. P_{coinc} was measured, using a cw-laser with 245 nW power, and 24 ± 2 coincidences per second were observed. Converting the pump power into number of photons per second numbers (9.56×10^{11} s^{-1}) we arrive at a coincidence probability, P_{coinc}, of $(2.5 \pm 0.2) \times 10^{-11}$.

Combining Eq. 4.2 and 4.3 leads to:

$$P_{triple} = \eta_{775} \frac{P_{coinc}}{\eta_{LP}^2 \, \eta_{duty}} \tag{4.4}$$

To arrive at the observed triplet rate, the trigger rate ($R_{trigger}$), and experimental values for the efficiency of the time acquisition card (η_{TAC}) and the SPDC bandwidth dependence (η_{cw}) have to be included, finally yielding:

$$R_{triple} = R_{trigger} \, \eta_{775} \frac{P_{coinc}}{\eta_{LP}^2 \, \eta_{duty}} \, \eta_{TAC} \, \eta_{cw} \tag{4.5}$$

Due to the internal deadtime, the time acquisition card only counted every second event and hence reduced the number of observed events by a factor of 2. Measurements of the PPLN waveguide have also shown that the acceptance of the down-conversion process with respect to the input wavelength is very small. The overall efficiency is hence reduced when broadband input photons (0.4 nm) are used as was the case in the C-SPDC measurements. The efficiency with such a broad pump was calculated to be 73% for optimal matching of the single photon wavelength and dropping to 55% when the input wavelength is 0.2 nm off. For the calculation of R_{triple}, a value of 0.67 ± 0.05 for η_{cw} is assumed here. Substituting the experimental values, as summarised in Table 4.1, in Eq. 4.5, a triplet rate of 5.6 ± 1.1 counts per hour is found.

4.8.2 Measurement of the down-conversion efficiency in the PPLN waveguide

By using the estimates for the various losses and efficiencies, the down-conversion probability per pump photon inside the waveguide of the secondary SPDC source, P_{SPDC}, was calculated from a coincidence measurement (Eq. 4.3) using 245 nW laser power and also from the measured triplets rate (Eq. 4.2) where 10^6 single photons per second were used. The laser pumping yields a P_{SPDC} of $(9.9 \pm 2.9) \times 10^{-6}$, compared to $(8.2 \pm 2.2) \times 10^{-6}$ for the single photon input. The down-conversion efficiency was also measured at a higher laser power of 1.1 mW. For this input, an SPDC power of 0.9 ± 0.1 nW could be detected at the output fiber of the waveguide using a standard power meter. Including the losses of the fiber couplings and the longpass filter, this measurement yields an P_{SPDC} of $(6.6 \pm 0.7) \times 10^{-6}$ for the waveguide.

$R_{trigger}$	$(8.70 \pm 0.05) \times 10^5$Hz
η_{D1}	0.45 ± 0.05
η_{775}	0.53 ± 0.06
P_{coinc}	$(2.5 \pm 0.2) \times 10^{-11}$
η_{LP}	0.50 ± 0.03
η_{duty}	0.01
η_{TAC}	0.5
η_{cw}	0.67 ± 0.05
η_{in}	0.50 ± 0.05
η_{out}	0.50 ± 0.05
η_{BS}	0.45 ± 0.05
η_{D2}	0.20 ± 0.02
η_{D3}	0.10 ± 0.01

Table 4.1: Experimental parameters used for the calculation of the triple coincidence rate (R_{triple}) and PPLN down-conversion efficiency (η_{SPDC}). Errors correspond to 1σ.

The agreement, within measurement errors, of the down-conversion efficiency obtained at input powers of 1.1 mW and 245 nW and for the single photon input is very good. This leads us to the conclusion that the SPDC probability is indeed constant over the observed power range, from 260 fW (10^6 pump photons per second) to 1 mW (10^{15} pump photons).

Chapter 5

Conclusion

In this thesis, we focused on different types of entangled photon sources. In Chapter 3, we demonstrated a highly efficient source of entangled photon pairs. This source uses a Sagnac interferometer configuration, which allows us to take full advantage of periodically poled materials. This source was then used for several experiments, related to quantum key distribution, cluster state quantum computing, remote state preparation, state discrimination, and entanglement-enhanced classical communication.

The next experiment, detailed in Chapter 4, was the first demonstration of a direct production of photon triplets. We cascaded two spontaneous parametric down-conversions to produce photon triplets, which were detected using their timing correlations. The SPDC phasematching conditions were used to confirm the presence of genuine photon triplets. This experiment was also the first observation of SPDC pumped at the single photon level, opening the way to a new regime of nonlinear optics.

The next step will be to demonstrate the entanglement of these photon triplets. To do this, we hope to entangle the photons in the polarization degree of freedom. This will require replacing each down-converter with a source of entangled photon pairs. For the first down-converter, we will again use a Sagnac interferometer configuration. However, unlike in the experiments described in this thesis, it will be operated far from degeneracy. The second down-converter will be replaced with an interferometric source of entangled photon pairs, in a Mach-Zehnder configuration. If this works, then this would be the same kind

of step forward for entangled triplets as the first single emitter scheme was for entangled pairs, as it would be the first direct production of entangled photon triplets. It could also be used to produce triggered Bell pairs, which are a useful tool for fundamental tests of quantum mechanics and linear optics quantum computing.

APPENDICES

Appendix A

Aligning the Sagnac Source

The aim of this appendix is to explain, as thoroughly as possible, the process of building and aligning a Sagnac source. It was written with the basic philosophy that it is better to include something which the reader already might already know than to risk omitting something which he does not. Consequently, some of these instructions might seem elementary for someone with experience working in optics.

A.1 Construction and rough alignment of the source

This section describes the initial construction of the Sagnac source, as shown in Figure 3.2, up to the point where down-converted photons are detected.

1. Start by setting up the the laser and the optical isolator. Note that the isolator is **not** optional. When the source is properly aligned, the pump beam is reflected back towards the laser cavity by the interferometer. A half-wave plate (HWP2) can be placed before the isolator in order to control the pump power.

2. Next, place the steering mirrors M1 and M2. Using these two mirrors and some irises, make sure that the beam is horizontal, and is aligned along the holes on the table.

3. Add the M3 mirror, and steer it so that the reflected beam is parallel to the table, and at 45° with the incoming beam. Then, place the lens so that it focuses the light onto the spot where you plan to have the crystal. The lens should be on a translation stage so that its position may be optimized later. Also keep in mind that the smaller the interferometer, the easier it will be to align mirrors M3 and M4.

4. The dichroic mirror can now be added. Since it does not have a back reflection, a good way to align it is to ensure that the reflection off its back face is perpendicular to the pump beam by using irises. The wave plates HWP1 and QWP1 can also be added now. The quarter-wave plate should be mounted so that it can be rotated around the vertical axis.

5. The next step is to add the PBS. It is important for the dichroic mirror to be already in place, as it will cause the beam to deviate a bit in the transverse direction. Make sure that the PBS is back-reflected (i.e. that the reflection coming from its front face is overlapping the incoming beam), and that the light coming out of the reflected port is traveling parallel to the table surface. Because the PBS is a central part of the interferometer, care should be taken on getting its alignment right the first time, as it is not something which can easily be adjusted later.

6. The last mirror, M4, is then added. It should be placed so that the intersection of the two beams coming from the PBS is on its surface, and angled such that at mirror M3, the two counter-propagating beams are superimposed. The tip and tilt of M3 are then adjusted in a similar way. It might be necessary to go back and forth and do this with both mirrors a few times. Essentially, the idea is simply to overlap the two counter-propagating beams at those two points, which ensures that they are overlapping everywhere in the interferometer.

7. The crystal can now go in. Ideally, all degrees of rotation should be available. In addition to this, it should be possible to translate the crystal along the direction of the beam. The other two directions of translation are useful to get the crystal in place, but are not critical for further alignment. For now, simply place the crystal in the center of the interferometer, and adjust the tip and tilt so that it is back-reflected.

8. The dual-wavelength half-wave plate (HWP3) can now be placed in the interferometer. It should be back-reflected, and its angle set to minimize the pump beam

intensity in output a of the PBS.

9. Next, the long-pass filters can be added, and then the couplers. The couplers can be roughly aligned by coupling light of the right wavelength into the single mode fibers. Simply make sure this light is overlapped with the pump beam, and focused near the crystal.

10. Now, it should be possible measure to some single photon counts. The maximum counts can be reached by walking the couplers. This completes the construction and rough alignment of the Sagnac source.

A.2 Precise alignment and fine-tuning of the Sagnac source

The following are the steps needed to align the Sagnac source. Some of these may have to be repeated a few times to get everything just right. They are also not all independent of each other, and so it can be necessary to go back and forth between the steps.

1. **Mirrors M3 and M4**. These are the first, and most important, elements to align. The goal is to have the two counter-propagating pump beams in the interferometer perfectly superimposed, so that the down-converted photons coming from both directions are coupled into the fibers. The procedure is as follows.

   (a) Set the wave plates HWP1 and QWP1 to produce horizontally polarized light, and walk both couplers (tip, tilt and translations) to have maximum *singles* counts for each. Once this is done, write down the position of all the translation stages.

   (b) Next, turn HWP1 to have vertically polarized light, and using *only translation* of the couplers, maximize *singles* for both. Write down the new positions of the translation stages.

   (c) Turn HWP1 to produce diagonally polarized light, and translate the couplers so that they are at the average of the positions obtained in steps (a) and (b).

(d) Finally, carefully adjust the mirrors M3 and M4 to maximize *coincidences*. It is usually necessary to walk them a bit to reach the maximum.

If the mirrors are fairly misaligned at the start (i.e. if there is a large difference between the positions found in (a) and (b)), it may be necessary to repeat this procedure a few times. When the alignment is good, translating the couplers in step (b) should lead to no noticeable improvement in the amount of counts measured. Let us add a few notes on this procedure:

- It is always good to make the final adjustment of the translation stages in the same direction to avoid backlash, particularly during later iterations of the alignment procedure.
- The maximum counts measured in (a) and (b) should be nearly equal; an unexplained large difference is indicative that something could be wrong. If, however, there is a known cause for this (for example, if the dual-wavelength half-wave plate works better for either the pump or the signal), then try to approximately compensate for the difference when setting HWP1 in (c). For example, if there are less counts when the pump is V polarized than when it is H polarized, set HWP1 so that the pump is a bit closer to V then to H.
- A slight variation of step (a) is to turn the dual-wavelength HWP by 22.5°, so that both photons from a pair may exit the PBS through the same port. Then, instead of walking the coupler to maximize singles, use a fiber beam splitter and maximize the number of coincidences between each of its outputs. This method ensures that the coupling is optimized for the photons originating from collinear down-conversion.

2. **Setting crystal temperature**. This is quite easy to do by simply using a spectrometer and setting the temperature to produce the desired wavelength. A useful trick is to turn HWP3 to 22.5° so that both idler and signal photons can be coupled into the same single mode fibre at the same time. That way, both of them may be monitored simultaneously.

3. **Dual wavelength HWP**. These can have a slightly different optical axis for different wavelengths. It is better to have it optimized for the signal than for the pump. Its

angle can be fine-tuned by slightly turning it to maximize coincidences, with HWP1 set to produce a horizontally polarized pump.

4. **Lens and crystal position**. The optimal position for the lens and crystal can be found with the same measurement. Start with the pump horizontally polarized. Then, translate the crystal along the beam's propagation direction. For each crystal position, find the maximum number of singles counts in one of the couplers by adjusting its position and focus. There should be an optimal position for the crystal, with the singles counts dropping when it is translated in either direction. Next, repeat the same measurement, but this time with the pump vertically polarized. The optimal crystal position is at the average of the two measured positions. The pump lens is in the right position if the optimal crystal position is the same for both directions.

5. **Interference filters**. To increase the coupling efficiency, interference filters may be added in front of each coupler. Obviously, these should only be added once the crystal's temperature has been set. If the transmission wavelength of the filters is slightly higher than that of the signal, slightly tilting these filters can help improve the transmission. This will also translate the beam, so it is necessary to "walk" the tilt of the filter, along with the appropriate translation of the coupler until the transmission is maximized.

A.3 Producing a Bell state

Once the source is aligned, it can then be set up to produce entangled states. To do this, the single mode fibres should be connected to wherever the Bell state will be sent. To set the source properly, we need to do polarization measurements on the photons in two bases, so a simple polarizer, or a PBS with a HWP are needed.

1. First the fibres can be connected to the experimental setup, passing through polarization controllers. The polarization controllers can be adjusted using the polarized single photons produced by the Sagnac source when the crystal is pumped in only one direction.

2. Next, set HWP1 to 22.5°, and the analyzers to the measurements in the horizontal/vertical basis where high correlations are expected. For example, if a $|\psi\rangle$ state is desired, the first analyzer could be set to H and the other to V. The rate of measured coincidental photon detections is then be measured.

3. The settings of both analyzers are inverted, and the rate of coincidental detections is again measured. Ideally, this should be equal to what was measured in the previous step. Otherwise, the angle of HWP1 should be tuned to make it that way. Simply go back and forth between the two pairs of settings, turning HWP1 slightly until the same rate of coincidences are measured for both settings.

4. Finally, change the analyzers to a setting from a different basis (for example the diagonal/anti-diagonal basis), where you want to have anti-correlations. Then, tilt QWP1 until the rate of measured coincidences are minimized. Et voilà, your desired Bell state is ready!

Appendix B

Calculating the theoretical phasematching curves

In this appendix, we show how we can calculate the theoretical phasematching curves shown in Figure 3.4. To obtain this plot, we first start with the phasematching Equation 1.32. We rewrite it in terms of wavelength, which gives us:

$$\frac{n_p}{\lambda_p} = \frac{n_s}{\lambda_s} + \frac{n_i}{\lambda_i} + \frac{1}{\Lambda} \tag{B.1}$$

where n_j represents the temperature dependant index of refraction for the pump, signal and idler. Because of energy conservation (Equation 1.23), we have $\lambda_s = (1/\lambda_p - 1/\lambda_i)^{-1}$. So we have to solve:

$$\frac{n_p}{\lambda_p} = n_i \left(\frac{1}{\lambda_p} - \frac{1}{\lambda_i} \right) + \frac{n_i}{\lambda_s} + \frac{1}{\Lambda}. \tag{B.2}$$

We now need to include the temperature dependance. For the parameters of this dependance, we based ourselves on [91], the source recommended by Alex Skliar from Raicol Crystals. First, the poling period will change slightly as the temperature changes. This change is given by:

$$\Lambda = \Lambda_0[1 + \alpha(T - 25°\mathrm{C}) + \beta(T - 25°\mathrm{C})^2] \tag{B.3}$$

with $\alpha = 6.7 \times 10^{-6\circ}$C and $\beta = 11 \times 10^{-9\circ}$C [91]. This however has only a small effect on the phasematching. The main contribution comes from the change in the refractive indices. In the PPKTP crystals that we use, the pump and signal are both polarized in the y direction, and the idler is polarized in the z direction. The room temperature values of the corresponding refractive indices are given by the following Sellmeier equations:

$$n_y^2 = A_y + \frac{B_y}{1 - C_y/\lambda^2} - D_y\lambda^2 \tag{B.4}$$

$$n_z^2 = A_z + \frac{B_z}{1 - C_z/\lambda^2} - \frac{D_z}{1 - E_z/\lambda^2} - F_z\lambda^2 \tag{B.5}$$

The value of the coefficients are indicated in Table B.1. The values for n_y and n_x are taken from [92] and [93] respectively.

Sellmeier coefficient	Value
A_y	2.19229
B_y	0.83547
C_y	0.04970
D_y	0.01621
A_z	2.12725
B_z	1.18431
C_z	0.0514852
D_z	0.6603
E_z	100.00507
F_z	9.68956×10^{-3}

Table B.1: KTP Sellmeier coefficients at room temperature

For the temperature dependance of the refractive index, Emanueli et al. [91] write the variation of the refractive index, Δn, as a parabolic function of the temperature T:

$$\Delta n(\lambda, T) = n_1(\lambda)(T - 25^\circ\text{C}) + n_2(\lambda)(T - 25^\circ\text{C})^2 \tag{B.6}$$

where the coefficient n_1 and n_2 are written as a third order polynomial of inverse wavelengths:

$$n_{1,2}(\lambda) = \sum_{m=0}^{3} \frac{a_m}{\lambda^m} \tag{B.7}$$

The values of the coefficients a_m for the x and y polarizations are included in Table B.2

	y polarization		z polarization	
	$n_1\,[10^{-6}]$	$n_2\,[10^{-8}]$	$n_1\,[10^{-6}]$	$n_2\,[10^{-8}]$
a_0	6.2897	-0.14445	9.9587	-1.1882
a_1	6.3061	2.2244	9.9228	10.459
a_2	-6.0629	-3.5770	-8.9603	-9.8136
a_3	2.6486	1.3470	4.1010	3.1481

Table B.2: Coefficients for KTP refractive index dependance on temperature

We now have the temperature dependance of every term in Equation B.2. If we substitute all of these in, along with the known poling period of the crystal and wavelength of the pump, we can then solve for the wavelength of the idler for any given temperature. The wavelength of the signal is then easy to calculate with Equation 1.23. We plot these over the same range of wavelengths as measured. The results are shown in Figure 3.4

Bibliography

[1] Stuart J. Freedman and John F. Clauser. Experimental test of local hidden-variable theories. *Phys. Rev. Lett.*, 28(14):938–941, Apr 1972. 3

[2] Edward S. Fry and Randall C. Thompson. Experimental test of local hidden-variable theories. *Phys. Rev. Lett.*, 37(8):465–468, Aug 1976. 3

[3] Alain Aspect, Philippe Grangier, and Gérard Roger. Experimental realization of Einstein-Podolsky-Rosen-Bohm gedankenexperiment: A new violation of Bell's inequalities. *Phys. Rev. Lett.*, 49(2):91–94, Jul 1982. 3

[4] Alain Aspect, Jean Dalibard, and Gérard Roger. Experimental test of Bell's inequalities using time- varying analyzers. *Phys. Rev. Lett.*, 49(25):1804–1807, Dec 1982. 3

[5] Z. Y. Ou and L. Mandel. Violation of Bell's inequality and classical probability in a two-photon correlation experiment. *Phys. Rev. Lett.*, 61(1):50–53, Jul 1988. 3, 16, 51

[6] Y. H. Shih and C. O. Alley. New type of Einstein-Podolsky-Rosen-Bohm experiment using pairs of light quanta produced by optical parametric down conversion. *Phys. Rev. Lett.*, 61(26):2921–2924, Dec 1988. 3, 16, 51

[7] P. R. Tapster, J. G. Rarity, and P. C. M. Owens. Violation of Bell's inequality over 4 km of optical fiber. *Phys. Rev. Lett.*, 73(14):1923–1926, Oct 1994. 3

[8] Paul G. Kwiat, Klaus Mattle, Harald Weinfurter, Anton Zeilinger, Alexander V. Sergienko, and Yanhua Shih. New high-intensity source of polarization-entangled photon pairs. *Phys. Rev. Lett.*, 75(24):4337–4341, Dec 1995. 3, 17, 32, 45, 51

[9] W. Tittel, J. Brendel, H. Zbinden, and N. Gisin. Violation of Bell inequalities by photons more than 10 km apart. *Phys. Rev. Lett.*, 81(17):3563–3566, Oct 1998. 3

[10] Gregor Weihs, Thomas Jennewein, Christoph Simon, Harald Weinfurter, and Anton Zeilinger. Violation of Bell's inequality under strict Einstein locality conditions. *Phys. Rev. Lett.*, 81(23):5039–5043, Dec 1998. 3

[11] Markus Aspelmeyer, Hannes R. Bohm, Tsewang Gyatso, Thomas Jennewein, Rainer Kaltenbaek, Michael Lindenthal, Gabriel Molina-Terriza, Andreas Poppe, Kevin Resch, Michael Taraba, Rupert Ursin, Philip Walther, and Anton Zeilinger. Long-distance free-space distribution of quantum entanglement. *Science*, 301(5633):621–623, 2003. 3

[12] K. Resch, M. Lindenthal, B. Blauensteiner, H. Böhm, A. Fedrizzi, C. Kurtsiefer, A. Poppe, T. Schmitt-Manderbach, M. Taraba, R. Ursin, P. Walther, H. Weier, H. Weinfurter, and A. Zeilinger. Distributing entanglement and single photons through an intra-city, free-space quantum channel. *Opt. Express*, 13(1):202–209, 2005. 3

[13] J. W. Pan, D. Bouwmeester, M. Daniell, H. Weinfurter, and A. Zeilinger. Experimental test of quantum nonlocality in three-photon Greenberger-Horne-Zeilinger entanglement. *Nature*, 403:515–519, 2000. 3

[14] Zhi Zhao, Tao Yang, Yu-Ao Chen, An-Ning Zhang, Marek Żukowski, and Jian-Wei Pan. Experimental violation of local realism by four-photon Greenberger-Horne-Zeilinger Entanglement. *Phys. Rev. Lett.*, 91(18):180401, Oct 2003. 3

[15] Philip Walther, Markus Aspelmeyer, Kevin J. Resch, and Anton Zeilinger. Experimental violation of a cluster state Bell inequality. *Phys. Rev. Lett.*, 95(2):020403, Jul 2005. 3

[16] Jonathan Lavoie, Rainer Kaltenbaek, and Kevin J Resch. Experimental violation of Svetlichny's inequality. *New Journal of Physics*, 11(7):073051, 2009. 3

[17] Artur K. Ekert. Quantum cryptography based on Bell's theorem. *Phys. Rev. Lett.*, 67(6):661–663, Aug 1991. 3

[18] D. S. Naik, C. G. Peterson, A. G. White, A. J. Berglund, and P. G. Kwiat. Entangled state quantum cryptography: Eavesdropping on the Ekert protocol. *Phys. Rev. Lett.*, 84(20):4733–4736, May 2000. 3

[19] W. Tittel, J. Brendel, H. Zbinden, and N. Gisin. Quantum cryptography using entangled photons in energy-time Bell states. *Phys. Rev. Lett.*, 84(20):4737–4740, May 2000. 3

[20] Thomas Jennewein, Christoph Simon, Gregor Weihs, Harald Weinfurter, and Anton Zeilinger. Quantum cryptography with entangled photons. *Phys. Rev. Lett.*, 84(20):4729–4732, May 2000. 3

[21] E Knill, R Laflamme, and GJ Milburn. A scheme for efficient quantum computation with linear optics. *NATURE*, 409(6816):46–52, JAN 4 2001. 3, 17

[22] Robert Raussendorf and Hans J. Briegel. A one-way quantum computer. *Phys. Rev. Lett.*, 86(22):5188–5191, May 2001. 3

[23] P Walther, KJ Resch, T Rudolph, E Schenck, H Weinfurter, V Vedral, M Aspelmeyer, and A Zeilinger. Experimental one-way quantum computing. *NATURE*, 434(7030):169–176, MAR 10 2005. 3

[24] Robert Prevedel, Philip Walther, Felix Tiefenbacher, Pascal Bohl, Rainer Kaltenbaek, Thomas Jennewein, and Anton Zeilinger. High-speed linear optics quantum computing using active feed-forward. *NATURE*, 445(7123):65–69, JAN 4 2007. 3

[25] Kai Chen, Che-Ming Li, Qiang Zhang, Yu-Ao Chen, Alexander Goebel, Shuai Chen, Alois Mair, and Jian-Wei Pan. Experimental realization of one-way quantum computing with two-photon four-qubit cluster states. *Phys. Rev. Lett.*, 99(12):120503, Sep 2007. 3

[26] Giuseppe Vallone, Enrico Pomarico, Paolo Mataloni, Francesco De Martini, and Vincenzo Berardi. Realization and characterization of a two-photon four-qubit linear cluster state. *Phys. Rev. Lett.*, 98(18):180502, May 2007. 3

[27] Daniel F. V. James, Paul G. Kwiat, William J. Munro, and Andrew G. White. Measurement of qubits. *Phys. Rev. A*, 64(5):052312, Oct 2001. 4, 5

[28] Nathan K. Langford. *Encoding, manipulating and measuring quantum information in optics*. PhD thesis, University of Queensland, 2007. 5

[29] C. K. Hong and L. Mandel. Theory of parametric frequency down conversion of light. *Phys. Rev. A*, 31(4):2409–2418, 1985. 7, 8

[30] Z. Y. Ou, L. J. Wang, and L. Mandel. Vacuum effects on interference in two-photon down conversion. *Phys. Rev. A*, 40(3):1428–1435, Aug 1989. 7

[31] R. Ghosh, C. K. Hong, Z. Y. Ou, and L. Mandel. Interference of two photons in parametric down conversion. *Phys. Rev. A*, 34(5):3962–3968, Nov 1986. 8, 9

[32] Morton H. Rubin, David N. Klyshko, Y. H. Shih, and A. V. Sergienko. Theory of two-photon entanglement in type-II optical parametric down-conversion. *Phys. Rev. A*, 50(6):5122–5133, Dec 1994. 8

[33] Hugues Guillet de Chatellus, Alexander V. Sergienko, Bahaa E. A. Saleh, Malvin C. Teich, and Giovanni Di Giuseppe. Non-collinear and non-degenerate polarization-entangled photon generation via concurrent type-I parametric downconversion in PPLN. *Opt. Express*, 14(21):10060–10072, 2006. 8

[34] Robert W. Boyd. *Nonlinear Optics*. Academic Press, 3 edition, 2008. 10

[35] J. A. Armstrong, N. Bloembergen, J. Ducuing, and P. S. Pershan. Interactions between light waves in a nonlinear dielectric. *Phys. Rev.*, 127(6):1918–1939, Sep 1962. 11

[36] David S. Hum and Martin M. Fejer. Quasi-phasematching. *Comptes Rendus Physique*, 8(2):180 – 198, 2007. Recent advances in crystal optics. 11, 14

[37] M. Yamada, N. Nada, M. Saitoh, and K. Watanabe. First order quasi phase matched LiNbO3 waveguide periodically poled by applying an external field for efficient blue second harmonic generation. *Applied Physics Letters*, 62(5):435 –436, 1993. 14

[38] Keiichi Edamatsu. Entangled photons: Generation, observation and characterization. *Japanese Journal of Applied Physics*, 46(11):7175–7187, 2007. 16

[39] Alessandro Fedrizzi. *Fundamental experiments with a high brightness source of entangled photons*. PhD thesis, Universitt Wien, 2008. 16

[40] Paul G. Kwiat, Philippe H. Eberhard, Aephraim M. Steinberg, and Raymond Y. Chiao. Proposal for a loophole-free bell inequality experiment. *Phys. Rev. A*, 49(5):3209–3220, May 1994. 17, 21

[41] T. E. Kiess, Y. H. Shih, A. V. Sergienko, and C. O. Alley. Einstein-Podolsky-Rosen-Bohm experiment using pairs of light quanta produced by type-II parametric down-conversion. *Phys. Rev. Lett.*, 71(24):3893–3897, Dec 1993. 17

[42] Paul G. Kwiat, Edo Waks, Andrew G. White, Ian Appelbaum, and Philippe H. Eberhard. Ultrabright source of polarization-entangled photons. *Phys. Rev. A*, 60(2):R773–R776, Aug 1999. 19, 32

[43] Yoshihiro Nambu, Koji Usami, Yoshiyuki Tsuda, Keiji Matsumoto, and Kazuo Nakamura. Generation of polarization-entangled photon pairs in a cascade of two type-i crystals pumped by femtosecond pulses. *Phys. Rev. A*, 66(3):033816, Sep 2002. 21

[44] Matthew Pelton, Philip Marsden, Daniel Ljunggren, Maria Tengner, Anders Karlsson, Anna Fragemann, Carlota Canalias, and Fredrik Laurell. Bright, single-spatial-mode source of frequency non-degenerate, polarization-entangled photon pairs using periodically poled KTP. *Optics Express*, 12:3573–3580, 2004. 21, 32

[45] A. V. Burlakov, M. V. Chekhova, O. A. Karabutova, D. N. Klyshko, and S. P. Kulik. Polarization state of a biphoton: Quantum ternary logic. *Phys. Rev. A*, 60(6):R4209–R4212, Dec 1999. 21

[46] Yoon-Ho Kim, Maria V. Chekhova, Sergei P. Kulik, Morton H. Rubin, and Yanhua Shih. Interferometric Bell-state preparation using femtosecond-pulse-pumped spontaneous parametric down-conversion. *Phys. Rev. A*, 63(6):062301, May 2001. 21

[47] Marco Fiorentino, Gaétan Messin, Christopher E. Kuklewicz, Franco N. C. Wong, and Jeffrey H. Shapiro. Generation of ultrabright tunable polarization entanglement without spatial, spectral, or temporal constraints. *Phys. Rev. A*, 69(4):041801, Apr 2004. 21

[48] W. Dür, G. Vidal, and J. I. Cirac. Three qubits can be entangled in two inequivalent ways. *Phys. Rev. A*, 62(6):062314, Nov 2000. 23

[49] A. Acín, D. Bruß, M. Lewenstein, and A. Sanpera. Classification of mixed three-qubit states. *Phys. Rev. Lett.*, 87(4):040401, Jul 2001. 23

[50] Dik Bouwmeester, Jian-Wei Pan, Matthew Daniell, Harald Weinfurter, and Anton Zeilinger. Observation of three-photon Greenberger-Horne-Zeilinger entanglement. *Phys. Rev. Lett.*, 82(7):1345–1349, Feb 1999. 23, 58

[51] Jian-Wei Pan, Matthew Daniell, Sara Gasparoni, Gregor Weihs, and Anton Zeilinger. Experimental demonstration of four-photon entanglement and high-fidelity teleportation. *Phys. Rev. Lett.*, 86(20):4435–4438, May 2001. 27

[52] J. G. Rarity and P. R. Tapster. Three-particle entanglement from entangled photon pairs and a weak coherent state. *Phys. Rev. A*, 59(1):R35–R38, Jan 1999. 27, 51, 52

[53] Huai-Xin Lu, Jun Zhang, Xiao-Qin Wang, Ying-De Li, and Chun-Yan Wang. Experimental high-intensity three-photon entangled source. *Phys. Rev. A*, 78(3):033819, Sep 2008. 27, 30

[54] N. Kiesel, M. Bourennane, C. Kurtsiefer, H. Weinfurter, D. Kaszlikowski, W. Laskowski, and M. Zukowski. Three-photon W-state. *J. of Mod. Opt.*, 50:1131–1138, 2003. 30, 58

[55] Manfred Eibl, Nikolai Kiesel, Mohamed Bourennane, Christian Kurtsiefer, and Harald Weinfurter. Experimental realization of a three-qubit entangled W state. *Phys. Rev. Lett.*, 92(7):077901, Feb 2004. 30

[56] Hideharu Mikami, Yongmin Li, Kyosuke Fukuoka, and Takayoshi Kobayashi. New high-efficiency source of a three-photon W state and its full characterization using quantum state tomography. *Phys. Rev. Lett.*, 95(15):150404, Oct 2005. 30

[57] N. Kiesel, C. Schmid, G. Tóth, E. Solano, and H. Weinfurter. Experimental observation of four-photon entangled Dicke state with high fidelity. *Phys. Rev. Lett.*, 98(6):063604, Feb 2007. 30

[58] Friedrich König, Elliott J. Mason, Franco N. C. Wong, and Marius A. Albota. Efficient and spectrally bright source of polarization-entangled photons. *Phys. Rev. A*, 71(3):033805, Mar 2005. 32

[59] Christopher E. Kuklewicz, Marco Fiorentino, Gaétan Messin, Franco N. C. Wong, and Jeffrey H. Shapiro. High-flux source of polarization-entangled photons from a periodically poled $ktiopo_4$ parametric down-converter. *Phys. Rev. A*, 69(1):013807, Jan 2004. 32

[60] Bao-Sen Shi and Akihisa Tomita. Generation of a pulsed polarization entangled photon pair using a sagnac interferometer. *Phys. Rev. A*, 69(1):013803, Jan 2004. 33

[61] Taehyun Kim, Marco Fiorentino, and Franco N. C. Wong. Phase-stable source of polarization-entangled photons using a polarization Sagnac interferometer. *Phys. Rev. A*, 73(1):012316, Jan 2006. 33

[62] F. N. C. Wong, J. H. Shapiro, and T. Kim. Efficient generation of polarization-entangled photons in a nonlinear crystal. *Laser Physics*, 16:15171524, 2006. 33

[63] Alessandro Fedrizzi, Thomas Herbst, Andreas Poppe, Thomas Jennewein, and Anton Zeilinger. A wavelength-tunable fiber-coupled source of narrowband entangled photons. *Opt. Express*, 15(23):15377–15386, 2007. 33, 38, 53

[64] *SPCM-AQ4C Single Photon Counting Module Array Datasheet*, 2005. 35

[65] Richard Jozsa. Fidelity for mixed quantum states. *JOURNAL OF MODERN OPTICS*, 41(12):2315–2323, DEC 1994. 41

[66] Valerie Coffman, Joydip Kundu, and William K. Wootters. Distributed entanglement. *Phys. Rev. A*, 61(5):052306, Apr 2000. 41

[67] D. N. Klyshko. Coherent photon decay in a nonlinear medium. *JETP Lett.*, 6:23–25, 1967. 51

[68] J. G. Rarity, P. R. Tapster, E. Jakeman, T. Larchuk, R. A. Campos, M. C. Teich, and B. E. A. Saleh. Two-photon interference in a Mach-Zehnder interferometer. *Phys. Rev. Lett.*, 65(11):1348–1351, Sep 1990. 51

[69] J. Brendel, N. Gisin, W. Tittel, and H. Zbinden. Pulsed energy-time entangled twin-photon source for quantum communication. *Phys. Rev. Lett.*, 82(12):2594–2597, Mar 1999. 51, 58

[70] A. Mair, A. Vaziri, G. Weihs, and A. Zeilinger. Entanglement of the orbital angular momentum states of photons. *Nature*, 412:312–316, 2001. 51

[71] Julio T. Barreiro, Nathan K. Langford, Nicholas A. Peters, and Paul G. Kwiat. Generation of hyperentangled photon pairs. *Phys. Rev. Lett.*, 95(26):260501, Dec 2005. 51

[72] S. Ramelow, L. Ratschbacher, A. Fedrizzi, N. K. Langford, and A. Zeilinger. Discrete tunable color entanglement. *Phys. Rev. Lett.*, 103(25):253601, Dec 2009. 51

[73] J. Persson, T. Aichele, V. Zwiller, L. Samuelson, and O. Benson. Three-photon cascade from single self-assembled InP quantum dots. *Phys. Rev. B*, 69(23):233314, Jun 2004. 51, 52

[74] D. M. Greenberger, M. A. Horne, A. Shimony, and A. Zeilinger. Bell theorem without inequalities. *Am. J. Phys.*, 58:1131–1143, 1990. 51, 52

[75] Timothy E. Keller, Morton H. Rubin, Yanhua Shih, and Ling-An Wu. Theory of the three-photon entangled state. *Phys. Rev. A*, 57(3):2076–2079, Mar 1998. 51, 52

[76] Suraj N. Gupta. Multiple photon production in electron-positron annihilation. *Phys. Rev.*, 96(5):1453, Dec 1954. 51, 52

[77] J. Douady and B. Boulanger. Experimental demonstration of a pure third-order optical parametricdownconversion process. *Opt. Lett.*, 29(23):2794–2796, 2004. 51, 52

[78] K. Bencheikh, F. Gravier, J. Douady, A. Levenson, and B. Boulanger. Triple photons: a challenge in nonlinear and quantum optics. *Comptes Rendus Physique*, 8:206–220, 2007. 51, 52

[79] H. C. Guo, Y. Q. Qin, and S. H. Tang. Parametric downconversion via cascaded optical nonlinearities in an aperiodically poled MgO : LiNbO3 superlattice. *App. Phys. Lett.*, 87:161101, 2005. 51, 52

[80] W. J. Munro and G. J. Milburn. Characterizing Greenberger-Horne-Zeilinger correlations in nondegenerate parametric oscillation via phase measurements. *Phys. Rev. Lett.*, 81(20):4285–4288, Nov 1998. 51

[81] M. Zukowski, A. Zeilinger, and H. Weinfurter. *Fundamental Problems in Quantum Theory: A Conference Held in Honour of Professor John A. Wheeler*, pages 91–102. NY Acad. Sci., 1995. 51

[82] Konrad Banaszek and Peter L. Knight. Quantum interference in three-photon down-conversion. *Phys. Rev. A*, 55(3):2368–2375, Mar 1997. 51

[83] A. Zeilinger, M.A. Horne, and D. M. Greenberger. Hiher-order quantum entanglement. *NASA Conf. Publ.*, 3135:73–81, 1992. 51

[84] Daniel E. Browne and Terry Rudolph. Resource-efficient linear optical quantum computation. *Phys. Rev. Lett.*, 95(1):010501, Jun 2005. 51

[85] Mark Hillery, Vladimír Bužek, and André Berthiaume. Quantum secret sharing. *Phys. Rev. A*, 59(3):1829–1834, Mar 1999. 51

[86] David C. Burnham and Donald L. Weinberg. Observation of simultaneity in parametric production of optical photon pairs. *Phys. Rev. Lett.*, 25(2):84–87, Jul 1970. 52, 55

[87] C. Kurtsiefer, M. Oberparleiter, and H. Weinfurter. Generation of correlated photon pairs in type-II parametric down conversion-revisited. *J. of Mod. Opt.*, 48:1997–2007, 2001. 53

[88] S. Tanzilli, H. De Riedmatten, W. Tittel, H. Zbinden, P. Baldi, M. De Micheli, D. B. Ostrowsky, and N. Gisin. Highly efficient photon-pair source using periodically poled lithium niobate waveguide. *Elec. Lett.*, 37(1):26–28, 2001. 53

[89] C. Kurtsiefer, P. Zarda, S. Mayer, and H. Weinfurter. The breakdown flash of silicon avalanche photodiodes-back door for eavesdropper attacks? *J. of Mod. Opt.*, 48:2039–2047, 2001. 55

[90] Paul G. Kwiat. Hyper-entangled states. *Modern Optics*, 44:2173–2184, 1997. 58

[91] Shai Emanueli and Ady Arie. Temperature-dependent dispersion equations for KTiOPO4 and KTiOAsO4. *Appl. Opt.*, 42(33):6661–6665, 2003. 72, 73

[92] Tso Yee Fan, C. E. Huang, B. Q. Hu, R. C. Eckardt, Y. X. Fan, Robert L. Byer, and R. S. Feigelson. Second harmonic generation and accurate index of refraction measurements in flux-grown KTiOPO4. *Appl. Opt.*, 26(12):2390–2394, 1987. 73

[93] K. Fradkin, A. Arie, A. Skliar, and G. Rosenman. Tunable midinfrared source by difference frequency generation in bulk periodically poled KTiOPO4. *Applied Physics Letters*, 74(7):914 –916, feb. 1999. 73